AGU ADVANCING EARTH AND SPACE SCIENCE

JGR Atmospheres

RESEARCH ARTICLE
10.1029/2022JD037260

Interdecadal to Multidecadal Variability of East Asian Summer Monsoon Over the Past Half Millennium

Feng Shi[1,2], Hugues Goosse[3], Jianping Li[4,5], Qiuzhen Yin[3], Fredrik Charpentier Ljungqvist[6,7,8], Tao Lian[9,10,11], Cheng Sun[12], Lin Wang[13], Zhiwei Wu[14,15], Juan Li[16], Sen Zhao[17], Chenxi Xu[1,2], Wei Liu[1,3], Ting Liu[9,10], Takeshi Nakatsuka[18,19], and Zhengtang Guo[1,2,20]

[1]Key Laboratory of Cenozoic Geology and Environment, Institute of Geology and Geophysics, Innovation Academy for Earth Science, Chinese Academy of Sciences, Beijing, China, [2]CAS Center for Excellence in Life and Paleoenvironment, Beijing, China, [3]Georges Lemaître Centre for Earth and Climate Research, Earth and Life Institute, Université Catholique de Louvain, Louvain-la-Neuve, Belgium, [4]Frontiers Science Center for Deep Ocean Multispheres and Earth System (FDOMES)/Key Laboratory of Physical Oceanography/Academy of the Future Ocean, Ocean University of China, Qingdao, China, [5]Laboratory for Ocean Dynamics and Climate, Pilot Qingdao National Laboratory for Marine Science and Technology, Qingdao, China, [6]Department of History, Stockholm University, Stockholm, Sweden, [7]Bolin Centre for Climate Research, Stockholm University, Stockholm, Sweden, [8]Swedish Collegium for Advanced Study, Uppsala, Sweden, [9]State Key Laboratory of Satellite Ocean Environment Dynamics, Second Institute of Oceanography, Ministry of Natural Resources, Hangzhou, China, [10]Southern Marine Science and Engineering Guangdong Laboratory (Zhuhai), Zhuhai, China, [11]School of Oceanography, Shanghai Jiao Tong University, Shanghai, China, [12]College of Global Change and Earth System Science (GCESS), Beijing Normal University, Beijing, China, [13]Center for Monsoon System Research, Institute of Atmospheric Physics, Chinese Academy of Sciences, Beijing, China, [14]Department of Atmospheric and Oceanic Sciences/Institute of Atmospheric Sciences, Fudan University, Shanghai, China, [15]Shanghai Key Laboratory of Meteorology and Health, Shanghai, China, [16]Earth System Modeling Center, Key Laboratory of Meteorological Disaster, Ministry of Education/Joint International Research Laboratory of Climate and Environment Change/Collaborative Innovation Center on Forecast and Evaluation of Meteorological Disasters, Nanjing University of Information Science and Technology, Nanjing, China, [17]Department of Atmospheric Sciences, University of Hawaii at Mānoa, Honolulu, HI, USA, [18]Research Institute for Humanity and Nature, Kyoto, Japan, [19]Graduate School of Environmental Studies, Nagoya University, Nagoya, Japan, [20]University of Chinese Academy of Sciences, Beijing, China

Abstract The East Asian summer monsoon (EASM) plays a crucial role for ecosystems and societies in East Asia past, present, and future. However, substantial uncertainties remain regarding EASM variability on interdecadal to multidecadal timescales because of the short length of instrumental data in East Asia. This study extended the EASM circulation index in the modern meteorological studies to the paleoclimate over the past half-millennium (1470–1998 CE) to reconcile the understanding of the EASM variability in paleoclimate and modern meteorological studies. The EASM index is reconstructed based on the common signal from the three main types of the proxy records (the tree rings, speleothems, and historical documentary data) related to EASM. The reconstructed EASM index captures the simultaneous changes of the "*Meiyu* precipitation" and the southwesterly anomalies in South China on interdecadal to multidecadal timescales, which is a dynamic pattern visible and well-documented in the modern meteorology. Analysis of the reconstructed EASM index suggests that the interdecadal to multidecadal EASM variability is closely associated with the Pacific-Japan teleconnection pattern, which acts as a bridge between the negative phase of the Pacific Decadal Oscillation and the anomalous anticyclonic circulation over the western North Pacific. It also indicates that the EASM variability over the recent 30 years (1992–2021 CE) falls within the range of natural variability over the past half-millennium.

Plain Language Summary The East Asian summer monsoon (EASM) determines the summer precipitation pattern in East Asia, home to approximately one-quarter of the world's population, and its interdecadal to multidecadal variability is thus of broad interest to both the scientific community and the public. However, it is difficult to reconstruct the EASM strength for the East Asia over the past centuries using only single types of precipitation-sensitive proxy records because the relationship between monsoon strength and precipitation intensity in China can vary between regions. We extended the EASM circulation index in the modern meteorological studies to the paleoclimate. This EASM index mainly reflect the simultaneous changes of the scarce/abundant summer precipitation belt along the Yangtze River valley extending to southern Japan,

Key Points:

- An East Asian summer monsoon (EASM) circulation index is reconstructed over the period 1470–1998 CE using 23 proxy records
- The EASM variability over the recent 30 years (1992–2021 CE) has not exceeded the range of natural variability over the past five centuries
- Multidecadal EASM variability is modulated by the Pacific Decadal Oscillation through the Pacific-Japan teleconnection pattern

Supporting Information:

Supporting Information may be found in the online version of this article.

Correspondence to:

F. Shi,
shifeng@mail.iggcas.ac.cn

Citation:

Shi, F., Goosse, H., Li, J., Yin, Q., Ljungqvist, F. C., Lian, T., et al. (2022). Interdecadal to multidecadal variability of East Asian summer monsoon over the past half millennium. *Journal of Geophysical Research: Atmospheres*, *127*, e2022JD037260. https://doi.org/10.1029/2022JD037260

Received 6 JUN 2022
Accepted 7 OCT 2022

Author Contributions:

Conceptualization: Feng Shi, Jianping Li
Data curation: Feng Shi
Formal analysis: Feng Shi, Tao Lian, Cheng Sun, Lin Wang, Juan Li, Sen Zhao, Wei Liu, Ting Liu
Funding acquisition: Feng Shi, Zhengtang Guo
Project Administration: Feng Shi, Zhengtang Guo
Resources: Feng Shi, Hugues Goosse, Qiuzhen Yin, Zhengtang Guo
Visualization: Feng Shi, Sen Zhao, Ting Liu
Writing – original draft: Feng Shi
Writing – review & editing: Feng Shi, Hugues Goosse, Jianping Li, Qiuzhen Yin, Fredrik Charpentier Ljungqvist, Tao Lian, Cheng Sun, Lin Wang, Zhiwei Wu,

Juan Li, Sen Zhao, Chenxi Xu, Wei Liu, Ting Liu, Takeshi Nakatsuka

and the northeasterly/southwesterly anomalies in South China on interdecadal to multidecadal timescales. The EASM variation was found to be linked to the anomalous sea surface temperature in the Pacific region that induced a counterclockwise/clockwise circulation in the Northwest Pacific region through the interrelated atmospheric anomalies that persist over the Pacific Ocean and the midlatitudes around Japan. The application of the reconstructed EASM index suggests that the EASM variability over the recent 30 years (1992–2021 CE) was not unprecedented over the past past-half millennium.

1. Introduction

The East Asian summer monsoon (EASM) has an enormous impact on agricultural and industrial water management for more than 1 billion people. Its interdecadal to multidecadal variability leads to periods of drought or flood across East Asia. Hence, great efforts have been made to explore the current EASM variability on interdecadal to multidecadal timescales (Chen et al., 2019; Ding et al., 2008; Huang et al., 2012; Zhou et al., 2009). However, previous studies focus on particular or a few decades-long transitions owing to the limitation of the short instrumental data. In particular, the EASM variability has exhibited a weakening tendency since the late 1970 s (Wang, 2001) and recovered since the early 1990 s (Liu et al., 2012). These short series affect the robustness of the conclusions on the mechanism controlling EASM decadal variability.

Paleoclimate proxy reconstruction could address this limitation of short instrumental data in East Asia. However, considerable uncertainties remain and the proxy reconstructions diverge in their interdecadal to multidecadal variability of the EASM over the past millennium (Shi et al., 2019; Zhang et al., 2010). There are two main reasons for this, one is caused by the proxy data itself, the other is the complex nature of the EASM.

Three main types of proxy records can be used to reconstruct the interdecadal to multidecadal EASM variability: tree ring records (Chen et al., 2020; Liu, Cai, et al., 2019), speleothem records (Tan et al., 2010; Zhang et al., 2008), and historical documentary data (Ge et al., 2008; Zheng et al., 2005), since some of them are significantly related to the instrumental Wang and Fan (1999)'s (WF) EASM circulation index (Figure 1). The indicators (width and $\delta^{18}O$) derived from the tree ring records have no dating error; they have furthermore a reasonably strong relationship with local precipitation variability (Xu, Zheng, et al., 2013; Yang et al., 2014), but may in some cases, depending on data treatment underestimate the low-frequency signals (multidecadal to long-term variability) (Fritts, 1976; Shi et al., 2020). Speleothem $\delta^{18}O$ records typically contain strong low-frequency signals (multidecadal to long-term variability) but with potentially larger dating uncertainties (Cheng et al., 2016). The dryness/wetness index over the last 500 years (Zhang, 1991) is the most commonly used historical documentary archive to record EASM variability as it is significantly related to the instrumental EASM index. Its results are also consistent with the "*Clear and Rain Records*" from the Qing Dynasty over the period 1723–1800 CE (Zhang & Wang, 1991). The dryness/wetness index only has five levels to reflect extreme rainfall. The "*Yu Xue Fen Cun*" record from eastern China since 1736 CE (Zheng et al., 2005) does not have this limitation, but its time span is too short to understand EASM variations over longer timescales.

The other issue is that the EASM has a complex spatial-temporal structure because it is influenced by changes in many regions, for example, the Pacific Ocean Basin, the Tibetan Plateau, and the Indian Ocean. To reflect this complex structure, there are four categories of EASM indices related to the tropics, subtropics, and midlatitudes structures, including the "east–west gradient" indices, the "north–south gradient" indices, the "southwest monsoon" indices, and the "South China Sea monsoon" indices (Wang et al., 2008). Different monsoon index definitions are selected for different scientific questions, for example, the South China Sea monsoon index is chosen to focus on the onset of the EASM, because the South China Sea monsoon is the root of the EASM (Chen & Chen, 1995) and the earliest onset of the EASM is over the South China Sea (Ding et al., 2004). Here, our goal is to capture the leading mode of EASM precipitation and circulation. This leading mode displays a southwest-northeast extended summer precipitation belt characterized by large anomalies from East China to Japan (called *Meiyu* in Chinese, *Baiu* in Japanese, and *Changma* in Korean) and southwesterly anomalies in South China associated to a large-scale 850 hPa anticyclonic anomaly extending from the northern South China Sea to the Philippine Sea (Li et al., 2020; Wang et al., 2008).

In addition, it is difficult to compare indices of present monsoon strength based on the circulation field for the instrumental period with past monsoon strengths, which is usually derived from a single proxy-based EASM

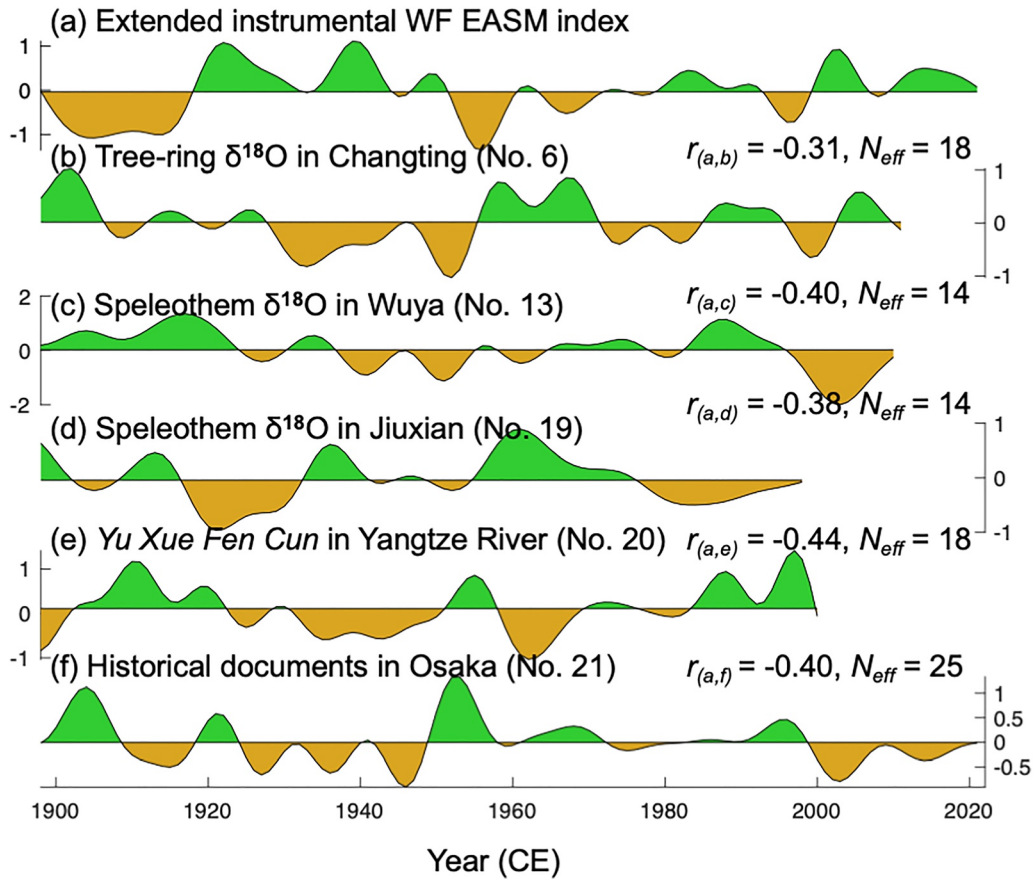

Figure 1. Comparison of the instrumental Wang and Fan (WF) East Asian summer monsoon (EASM) index over the period 1898–2021 CE (a) with the three types of proxy records (the tree ring $\delta^{18}O$ records in Changting (No. 6) (Xu, Zheng, et al., 2013) (b), and the speleothem $\delta^{18}O$ records in the Wuya cave (No. 13) (Tan et al., 2020) (c), and in the Jiuxian cave (No. 19) (Cai et al., 2010) (d), the Yu Xue Fen Cun in Yangtze River region (No. 20) (Ge et al., 2008) (e), and the historical documents in Osaka (No. 21) (Mizukoshi, 1993) (f)). *r* is the correlation coefficient between the instrumental EASM index with the proxy records during the common period. N_{eff} is the effective degree of freedom in the common period. All correlations are significant at the 90% level based on a one-tailed Student's *t*-test.

reconstruction (Zhang et al., 2010). This deficiency has resulted in misunderstanding and confusion between the modern meteorological and the paleoclimate monsoon research communities (Wang et al., 2008).

In response to these problems, we first reconstruct a EASM circulation index using the multi-proxy synthesis that can be directly compared with the EASM index in the modern meteorological studies. Multi-proxy syntheses are often used to capture the large-scale climate variability including the hemispheric mean temperature (Mann et al., 2008; Neukom et al., 2019; Shi et al., 2013), the North Atlantic Oscillation (Ortega et al., 2015), and the Southern Annular Mode index (Abram et al., 2014). Following a similar approach, the three types of proxy records (tree rings, speleothems, and historical documentary data) are integrated to deal with the divergence between the proxy records. Moreover, we reconstruct the EASM circulation index during, and prior to, the instrumental period to reconcile meteorological and paleoclimatological understandings of the EASM. Finally, the analogies of the recent 30-year of variability of EASM are used to explore the position of the current changes.

2. Data and Methods

In this study, 23 proxy records are compiled and processed employing the optimal information extraction (OIE) method to reconstruct the EASM circulation index over the past half millennium. Then, data assimilation is applied to analyze the mechanism responsible for the EASM variability.

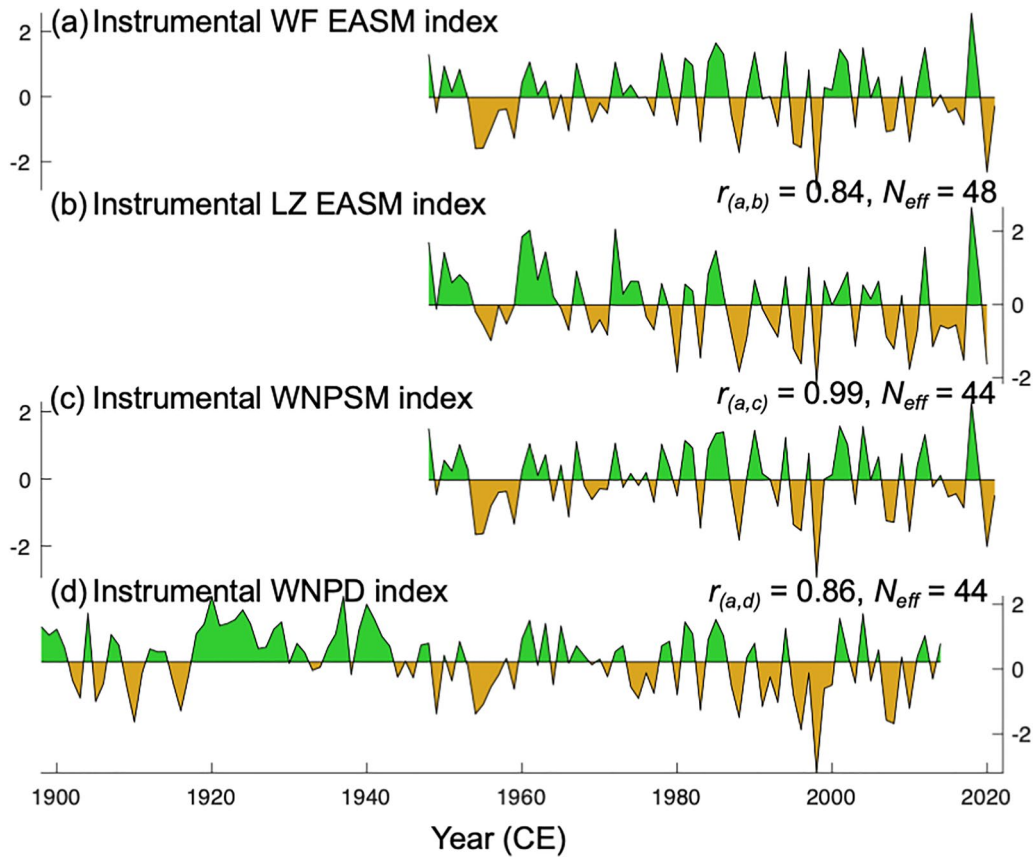

Figure 2. Comparison of the instrumental Wang and Fan (WF) East Asian Summer Monsoon (EASM) index (Wang & Fan, 1999) (black) with the instrumental Li and Zeng (LZ) EASM index (Li & Zeng, 2002) (red, (a)), the Western North Pacific Summer Monsoon (WNPSM) index (Wang et al., 2001) (red, (b)), and the Western North Pacific Directional (WNPD) index (Vega et al., 2018) (red, (b)). The instrumental WF index is defined as a north–south gradient of the zonal wind at 850 hPa (the U850 in (5–15°N, 90–130°E) minus U850 in (22.5–32.5°N, 110–140°E) using the NCEP1 Reanalysis data set (Wang & Fan, 1999). The instrumental LZ index is defined as an area-averaged seasonally (June–August, JJA) dynamical normalized seasonality within the domain (10–40°N, 110–140°E) (Li & Zeng, 2002). The WNPSM index is originally defined as a north–south gradient of the zonal wind at 850 hPa (the U850 in (5–15°N, 100–130°E) minus U850 in (20–30°N, 110–140°E) using the NCEP1 Reanalysis data set (Wang et al., 2001). The WNPD index is defined as the percentage of days in a month with prevailing wind blowing from the west/east in the area (20–30°N, 110–140°E)/(5–15°N, 100–130°E) (Vega et al., 2018). r is the correlation coefficient between the instrumental WF EASM index with other EASM indices during the common period. N_{eff} is the effective degree of freedom in the common period. All correlations are significant at the 90% confidence level based on a one-tailed Student's t-test.

2.1. Data

Our reconstructed target is the instrumental WF EASM circulation index over the period 1948–2021 CE (Figure 2a), which is defined by a north–south gradient of the zonal wind at 850 hPa (the U850 in (5–15°N, 90–130°E) minus U850 in (22.5–32.5°N, 110–140°E) using the NCEP Reanalysis data set (Wang & Fan, 1999). The reason for employing this target is that the WF index can capture the first leading mode of summer precipitation and the three-dimensional circulations associated with EASM over the instrumental period with 94.09% explained variance for 1979–2006 CE (Wang et al., 2008). This WF EASM index is also significantly related to the typical southwest monsoon index defined using the area-averaged seasonally (June–August, JJA) 850 hPa southwesterly winds (r = 0.84) within the domain (10–40°N, 110–140°E) (Li & Zeng, 2002) (Figure 2b). Moreover, the reconstructed target is extended to 1898 CE based on the strong correlations between the WF index and the Western North Pacific Summer Monsoon (WNPSM) index (Wang et al., 2001) (Figure 2c), and the WF index and the Western North Pacific Directional (WNPD) index (Vega et al., 2018) (Figure 2d) to enhance the robustness of the reconstruction. The WNPSM index is originally defined as a north–south gradient of the zonal wind at 850 hPa (the U850 in the area (5–15°N, 100–130°E) minus U850 in the area (20–30°N, 110–140°E) (Wang

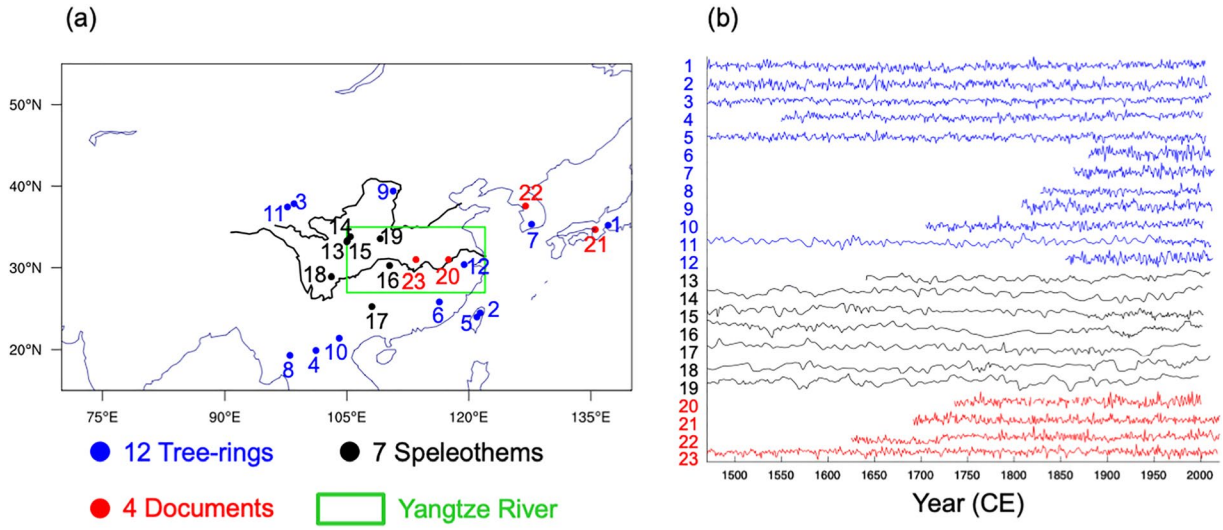

Figure 3. The geographical distribution (a) of 23 proxy records and their time series (b). The blue points and lines are the tree-ring records, the black points and lines are the speleothem records, the red points and lines are the historical documents, and the green box indicates the middle and lower Yangtze River region (27–35°N, 105–122°E) in China.

et al., 2001), and then continuously reconstructed to 1898 CE based on historical wind direction observations (Vega et al., 2018). The WNPD index is defined as the percentage of days in a month with prevailing wind blowing from the west/east in the area (20–30°N, 110–140°E)/(5–15°N, 100–130°E) (Vega et al., 2018).

The criteria for proxy selection are (a): The data developer utilized the proxy record to characterize EASM variability; (b) the indicators can capture the EASM variability or precipitation variability; (c) the timespan of the proxy record exceeds 100 years, and it covers the 1880–1998 CE initial calculation period; (d) the temporal resolution of the proxy record is less than 10 years or better. We screened 23 proxy records including 2 tree ring width chronologies (Sun et al., 2021; Yang et al., 2014) and 10 tree ring $\delta^{18}O$ chronologies (Liu, Cobb, et al., 2017; Liu, Wang, et al., 2019; Nakatsuka et al., 2020; Sano et al., 2012; Seo et al., 2019; Xu, Sano, et al., 2013; Xu, Zheng, et al., 2013; Xu et al., 2015; Xu et al., 2016; Yang et al., 2021), 7 speleothem $\delta^{18}O$ records (Cai et al., 2010; Hu et al., 2008; Tan et al., 2010, 2018, 2020; Wang et al., 2005; Zhang et al., 2008), and 4 historical documentary records (Ge et al., 2008; Mizukoshi, 1993; Shi, Zhao, et al., 2017; Wang et al., 2021) (Figure 3). The historical documentary records are in the monsoon core area, and the natural proxy records are mainly distributed in the monsoon fringe area. The detailed information about the 23 proxy records is provided in Table 1. The regional precipitation is used in mechanistic models to shape tree growth (Vaganov et al., 2011) and oxygen isotopes variability (Danis et al., 2012). In addition, the tree ring width records in monsoon Asia are significantly correlated with the instrumental Asian summer monsoon index (Shi et al., 2014; Shi, Fang, et al., 2017), and the tree ring $\delta^{18}O$ records in monsoon Asia are furthermore significantly related to the instrumental Asian summer monsoon oxygen isotope index (Xu et al., 2021). Moreover, speleothem $\delta^{18}O$ is demonstrated to reflect the EASM in climate model simulations (Liu et al., 2014) and instrumental observation (Duan et al., 2016; X. Li et al., 2017). All speleothem $\delta^{18}O$ records are interpolated to the annual resolution using the Piecewise Cubic Hermite Interpolating Polynomial method, which connects points flatter than the more commonly used spline interpolation method to avoid artificial local extrema (Fritsch & Carlson, 1980). The four historical documentary records include the length of *Meiyu* from the "*Yu Xue Fen Cun*" record (Ge et al., 2008), the summer (June to July) precipitation in Osaka (Mizukoshi, 1993), the summer (June to September) precipitation in Seoul (Kim & Ha, 2021), and the extended summer (May–September, MJJAS) precipitation in the middle and lower reaches of the Yangtze River region (27–35°N, 105–122°E) (Shi, Zhao, et al., 2017).

A recent data assimilation-based climate data set (Shi et al., 2019) is used to explore the atmospheric circulation associated with EASM variability and the possible mechanism responsible for the changes. The particle filter is used frequently as data assimilation method (Dubinkina et al., 2011; Lyu et al., 2021; van Leeuwen, 2009), in particular to reconstruct past climate variation and obtain this data assimilation-based climate data set (Shi et al., 2019). In the procedure, the ensemble members from the Community Earth System Model (CESM) Last

Journal of Geophysical Research: Atmospheres
10.1029/2022JD037260

Table 1
The Information of 23 Proxy Records

No.	Lat.	Lon.	Site	Country	Start year	End year	Res. (year)	Proxy	Archive type	Repo.	Reference doi	Original data URL
1	34.6°–35.8°	135.7°–138.5°	Central Japan	Japan	1	2005	1	$\delta^{18}O$	Tree-ring	ITRDB	10.5194/cp-16-2153-2020	https://www.ncdc.noaa.gov/paleo/study/28832
2	24.5°	121.4°	Taiwan	China	1190	2007	1	$\delta^{18}O$	Tree-ring	ITRDB	10.1038/ncomms15386	https://www.ncdc.noaa.gov/paleo/study/28417
3	37.0°–38.7°	97°–100°	Northeastern TP	China	1	2011	1	Width	Tree-ring	ITRDB	10.1073/pnas.1319238111	https://www.ncdc.noaa.gov/paleo/study/16034
4	19.9°	101.2°	Northern Laos	Laos	1550	2002	1	$\delta^{18}O$	Tree-ring	NaN	10.1016/j.palaeo.2013.06.025	NaN
5	24°	121°	Taiwan	China	1259	2006	1	Width	Tree-ring	ITRDB	10.1029/2020JD033603	https://www.ncdc.noaa.gov/paleo/study/32932
6	25.9°	116.4°	Changting	China	1880	2011	1	$\delta^{18}O$	Tree-ring	NaN	10.1002/2013JD019803	NaN
7	35.3°	127.7°	Jirisan National Park	Korea	1864	2015	1	$\delta^{18}O$	Tree-ring	ITRDB	10.1016/j.dendro.2019.125626	https://www.ncdc.noaa.gov/paleo/study/27111
8	19.3°	98°	Northwest Thailand	Thailand	1828	2000	1	$\delta^{18}O$	Tree-ring	NaN	10.1016/j.jhydrol.2015.02.037	NaN
9	39.4°	110.7°	Ordos Plateau	China	1808	2012	1	$\delta^{18}O$	Tree-ring	ITRDB	10.1029/2019JD030512	https://www.ncdc.noaa.gov/paleo/study/27191
10	21.4°	104.1°	Mu Cang Chai	Vietnam	1705	2004	1	$\delta^{18}O$	Tree-ring	Asia2k	10.1029/2012JD017749	NaN
11	37.5°	97.7°	Delingha	China	1	2011	3	$\delta^{18}O$	Tree-ring	ITRDB	10.1073/pnas.2102007118	https://www.ncdc.noaa.gov/paleo/study/33654
12	30.4°	119.4°	Zhejiang	China	1855	2013	1	$\delta^{18}O$	Tree-ring	NaN	10.1002/2015JD023610	NaN
13	33.8°	105.4°	Wuya	China	509	2010	4	$\delta^{18}O$	Speleothem	NCEI-NOAA	10.1029/2020GL090273	https://www.ncdc.noaa.gov/paleo/study/31592
14	33.4°	105.7°	Huangye	China	138	2002	6	$\delta^{18}O$	Speleothem	NCEI-NOAA	10.1177/0959683610378880	https://www.ncdc.noaa.gov/paleo/study/11177
15	33.2°	105.0°	Wanxiang	China	192	2003	3	$\delta^{18}O$	Speleothem	NCEI-NOAA	10.1126/science.1163965	https://www.ncdc.noaa.gov/paleo/study/8629
16	30.3°	110.3°	Heshang	China	1	2002	3	$\delta^{18}O$	Speleothem	NCEI-NOAA	10.1016/j.epsl.2007.10.015	https://www.ncdc.noaa.gov/paleo/study/6095
17	25.3°	108.1°	Dongge	China	1	2000	4	$\delta^{18}O$	Speleothem	NCEI-NOAA	10.1126/science.1106296	https://www.ncdc.noaa.gov/paleo/study/5439
18	28.9°	103.1°	Shenqi	China	1	2010	5	$\delta^{18}O$	Speleothem	NCEI-NOAA	10.1016/j.quascirev.2018.07.021	https://www.ncdc.noaa.gov/paleo/study/24710

Journal of Geophysical Research: Atmospheres

10.1029/2022JD037260

Table 1
Continued

No.	Lat.	Lon.	Site	Country	Start year	End year	Res. (year)	Proxy	Archive type	Repo.	Reference doi	Original data URL
19	33.6°	109.1°	Jiuxian	China	1	1998	4	$\delta^{18}O$	Speleothem	NCEI-NOAA	10.1016/j.epsl.2009.12.039	https://www.ncdc.noaa.gov/paleo/study/9742
20	30°–32°	112°–123°	Middle and Lower Reaches of Yangtze River	China	1736	2000	1	Yu Xue Fen Cun	Documentary	NaN	10.1007/s11434-007-0440-5	NaN
21	34.7°	135.5°	Osaka	Japan	1692	2020	1	NaN	Documentary	NaN	10.5026/jgeography.102.2_152	NaN
22	37.6°	127.0°	Seoul	Korea	1625	2020	1	NaN	Documentary	NaN	10.12197/2021GA013	http://www.geophys.ac.cn/ArticleData/20210608RainfallDataByWang.zip
23	27°–35°	105°–122°	Middle and Lower Reaches of Yangtze River	China	1470	2000	1	Drought and Flood index	Documentary and Tree-ring	NCEI-NOAA	10.5194/cp-13-1919-2017	https://www.ncdc.noaa.gov/paleo/study/23056

Note. No. = Numero sign. Lat. = Latitude. Lon. = Longitude. Res. = Resolution. Repo. = Repository. NaN = Missing values. ITRDB = International Tree-Ring Data Bank. NCEI-NOAA = National Centers for Environmental Information in National Oceanic and Atmospheric Administration.

Millennium Ensemble (CESM-LME) simulation (Otto-Bliesner et al., 2016) are considered as the particles. A weight is calculated for each particle depending on its likelihood computed from the difference between the precipitation obtained in this simulation and the proxy-based precipitation for China from the extended summer MJJAS precipitation field reconstruction using the OIE method (Shi, Zhao, et al., 2017). This weight is then used for all the simulated variables to obtain the other reconstructions for each of them (e.g., wind velocity and temperature) from the CESM-LME simulation, the mean reconstruction being simply the weighted mean of the particles (Shi et al., 2019). This data assimilation-based reconstruction can accurately reproduce the precipitation pattern and corresponding circulation information (Shi et al., 2019). Correspondingly, the data assimilation-based zonal wind anomalies at 850 hPa is used to calculate the data assimilation-based WF EASM index, which is compared with the proxy-based reconstructed WF EASM index to define the strong/weak monsoon events.

2.2. Methods

The OIE method (Neukom et al., 2019; Shi et al., 2014) is used to reconstruct the EASM index. The OIE method was derived from the traditional Composite Plus Scale method (Bradley & Jones, 1993), and inspired by the local (LOC) method (Christiansen, 2011), a Bayesian framework (Tingley & Huybers, 2010), and the generalized likelihood uncertainty estimation (GLUE) method (Wang, Hoffmann, et al., 2017). The main advantage of the OIE method is to efficiently retain low-frequency climate signals, since the nonlinear process of proxy records in response to climate is considered based on Bayesian theory (Shi et al., 2021). The specific implementation of the method is given as follows:

2.2.1. Filtering the Predictors

All proxy records and the instrumental EASM index are filtered by a 6th-order bandpass Butterworth filter to obtain the interdecadal to multi-decadal variability. The cut-off frequency is [1/101, 1/9]. All proxy records are first normalized to zero mean and one standard deviation.

2.2.2. Assigning the Predictors

As the selected predictors have different time periods, we thus divided the datasets into five spans: 1880–1998 CE (23 records), 1736–1998 CE (18 records), 1692–1998 CE (16 records), 1550–1998 CE (13 records), 1470–1998 CE (12 records). Each data set is used individually to obtain five EASM reconstructions as five members of the final ensemble reconstruction.

2.2.3. Regressing the Predictors

Each data set is calibrated against the instrumental WF EASM index using the partial least squares regression and ridge regression with the calibration/verification period (1898–1970 CE/1971–1998 CE). The two regression methods are used to reduce the uncertainty of the regression methods. Then, the regressed result is used as one composited proxy record and it is again calibrated using the Ensemble local regression method (Shi et al., 2012). This assumes that the regression coefficients are random variables that obey a uniform distribution with a range between the traditional classical calibration (direct regression) and the inverse calibration (indirect regression) (Shi, Zhao, et al., 2017; Shi et al., 2021). This process is used to generate 1000 realizations using the generalized likelihood uncertainty estimation method (Blasone et al., 2008; Wang, Hoffmann, et al., 2017). Finally, the median value of all ensemble members is considered as the final reconstruction.

2.2.4. Estimating the Uncertainty

The traditional verification variables (including the reduction of error, the coefficient of efficiency, the squared Pearson correlation coefficient, the root mean square error (RMSE), and the RMSE skill score) are used to test the accuracy of the reconstructions (verification skill) for each member.

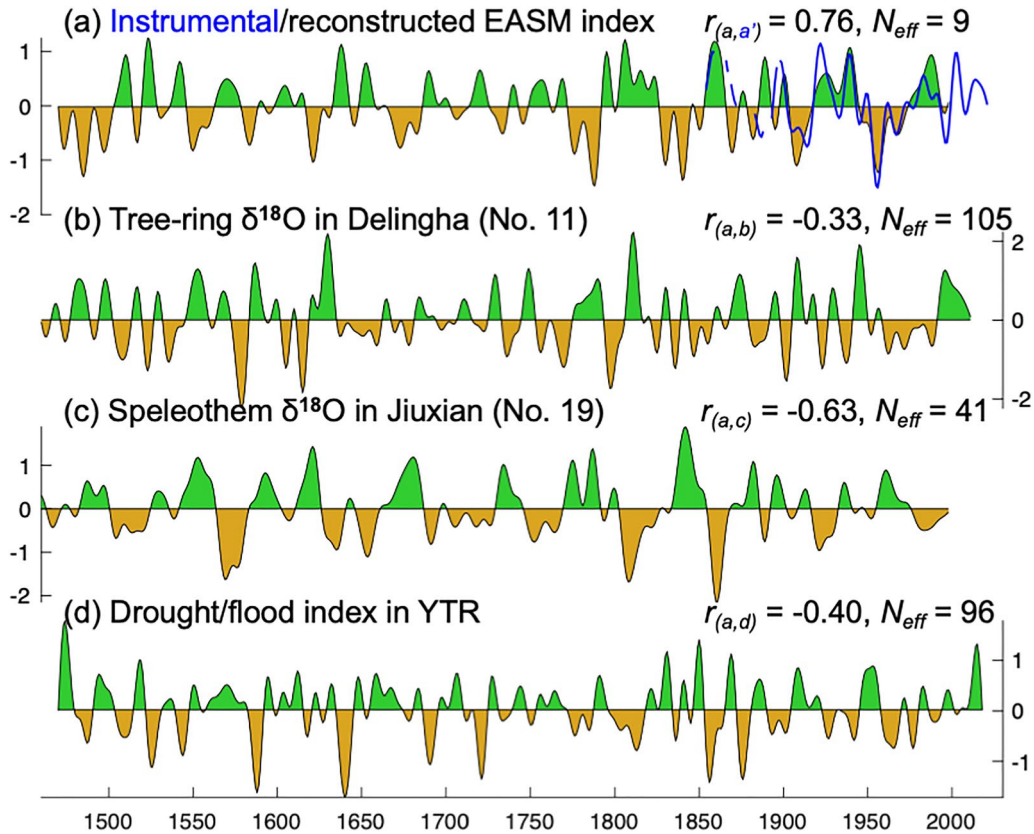

Figure 4. Comparison of the instrumental (blue)/reconstructed East Asian summer monsoon index (a) with the three long proxy records (the tree ring $\delta^{18}O$ record (No. 11) (Yang et al., 2021) (b), the speleothem $\delta^{18}O$ record in Jiuxian cave (No. 19) (Cai et al., 2010) (c), and the Dryness/Wetness index in the middle and lower Yangtze River region (27–35°N, 105–122°E) in China (Chinese Academy of Meteorological Science, 1981) (d)). r is the correlation coefficient between the reconstructed EASM index with the proxy records during the common period. N_{eff} is the effective degree of freedom in the common period. All correlations are significant at the 90% level based on a one-tailed Student's t-test.

The statistical significance of the correlation between two time series is accessed via a one-tailed Student's t-test using the effective number of degrees of freedom (N_{eff}), which in each correlation period is estimated according to equation 30 in Bretherton et al. (1999):

$$N_{\text{eff}} = \frac{N}{\sum_{\tau=-(N-1)}^{N-1} (1 - |\tau|/N)\rho_\tau^X \rho_\tau^Y} \quad (1)$$

where N is the length of the correlation period, ρ_τ^X and ρ_τ^Y are autocorrelation coefficients of two sampled time series X and Y at time lag τ, respectively.

3. Results

3.1. Comparison of the Reconstructed EASM Index With Other Reconstructions

The reconstructed EASM circulation index over the period 1470–1998 CE is shown in Figure 4a. It is significantly correlated with the instrumental EASM index (r = 0.76, N_{eff} = 9) over the whole calculation period (1898–1998 CE). The EASM reconstruction passes the traditional verification testing since the median reduction of error (0.37) and the median coefficient of efficiency (0.47) are both higher than zero. The performance of the EASM reconstruction is also good with a small median RMSE (0.36) and a median RMSE skill score (0.41). In addition, our reconstructed EASM index shows strong agreement with three long records including a tree ring $\delta^{18}O$ record in Delingha (Yang et al., 2021) (Figure 4b), a speleothem $\delta^{18}O$ record in Jiuxian cave

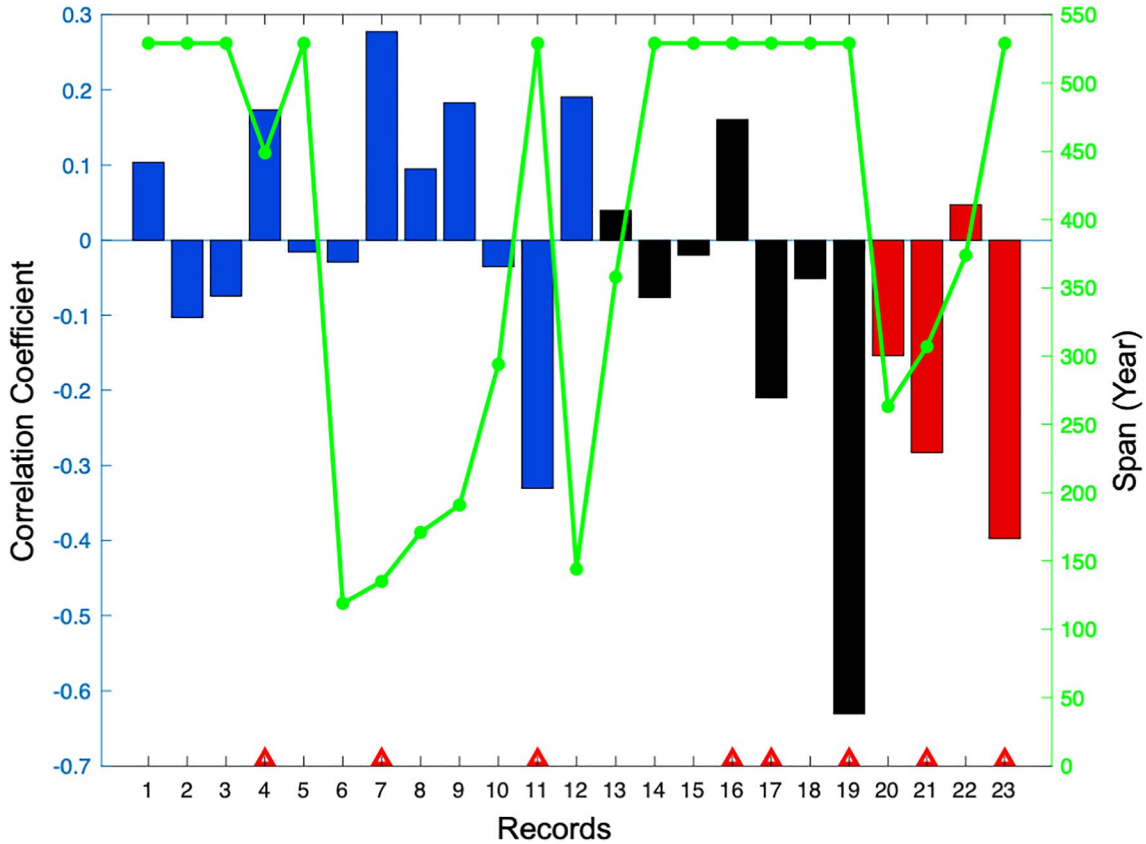

Figure 5. Relationship between the reconstructed East Asian summer monsoon (EASM) index with 23 proxy records (the tree ring records (blue), the speleothem records (black), and the historical documents (red)). The green line is the time span of each proxy record. The red triangles indicate the correlations between the reconstructed EASM index and the proxy records at the 90% confidence level.

(Cai et al., 2010) (Figure 4c), and a mean Dryness/Wetness index from the middle and lower Yangtze River region (27–35°N, 105–122°E) in China (Chinese Academy of Meteorological Science, 1981) (Figure 4d). This supports that our reconstruction represents the common signal from the three types of proxy records related to EASM.

A comparison of the reconstructed EASM index with the two types of natural proxy records shows no consistent relationship between a type of proxy records and the reconstructed EASM circulation index, especially for the tree-ring records (Figure 5). Most of the speleothem $\delta^{18}O$ records are negatively correlated with the EASM index, but there are two exceptions: the records in the Wuya cave (Tan et al., 2020) and in Heshang cave (Hu et al., 2008) (Figure 5). Observations suggest that the speleothem $\delta^{18}O$ records in China mainly respond to the isotope changes of atmospheric precipitation $\delta^{18}O$ outside the caves (Duan et al., 2016), which is primarily affected by the isotopic composition of source water. The upstream depletion of source water is linked with the southerly monsoon winds in Asia (Liu et al., 2014). Meanwhile, the tree-ring $\delta^{18}O$ records are mainly controlled by the isotopic composition of source water absorbed by roots, and the evaporative enrichment caused by leaf transpiration and linked to the effect of local hydroclimate (Field et al., 2022; Lavergne et al., 2017; Roden et al., 2000). These two contributions both have significant influences on the tree-ring $\delta^{18}O$ variability in East Asia (An et al., 2014; Li et al., 2011; Liu, Liu et al., 2017; Xu et al., 2015, 2021). Thus, the variabilities of the tree-ring $\delta^{18}O$ records in Asia are less consistent than that of the speleothem $\delta^{18}O$ records. Conversely, except that the precipitation in Seoul from historical documentary data is not significantly related to the EASM index, the other three historical documentary series located in the monsoon core region are consistently negatively related to the EASM index. The annual precipitation record in Seoul contains the *Meiyu* and post-*Meiyu* precipitation variability. The latter may not be well correlated with EASM variability, as it is associated with the Eurasian pattern where the rainfall comes from polar front/mesoscale convective activities (Wang et al., 2007).

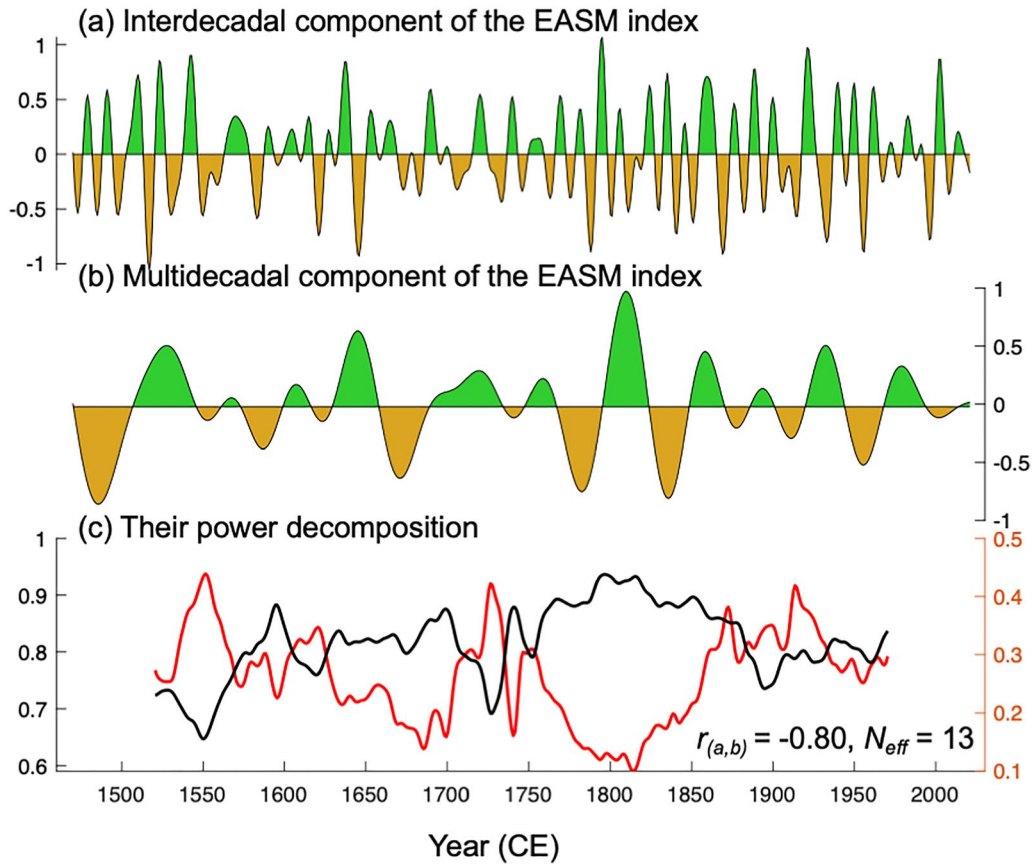

Figure 6. Comparison of the interdecadal component (a) and the multidecadal component (b) of the reconstructed East Asian summer monsoon index. The evolutionary spectral powers (c) using the power decomposition analysis (Li, Huang, et al., 2016) of the interdecadal component (black) and the multidecadal component (red). r is the correlation coefficient of the evolutionary spectral powers of the two components. N_{eff} is the effective degree of freedom in the common period.

The reconstructed EASM variability is decomposed in an interdecadal component (Figure 6a) and an multidecadal component (Figure 6b) using the 6th-order bandpass Butterworth filter. Following the previous studies (Mann et al., 1995; Shi, Fang, et al., 2017), the cut-off frequency for the interdecadal component and the multidecadal component are [1/35, 1/9] and [1/101, 1/35], respectively. The interdecadal component of the reconstructed EASM index over the period 1470–2021 CE explains ∼55.4% of the total variance, this number is slightly influenced by the filter method, but the standard deviation of the interdecadal component is a little larger than that of the multidecadal component, which is independent of the filter method. Moreover, the interdecadal component of the reconstructed EASM index is insignificantly related to the multidecadal component, and the evolutionary spectral powers of the two components have a distinct trade-off relationship (Figure 6c), because the correlation coefficient between the evolutionary spectral powers of the two components is $r = -0.80$.

3.2. Atmospheric Circulation of the EASM Index

To explore the physical processes at the origin of the reconstructed EASM variability, we selected 14/17 strong/weak EASM events from the common interdecadal to multidecadal component of the proxy reconstructed EASM index and the data assimilation based EASM index (Figure 7a), even though their correlation is not stable (Figure 7b). The screening criterion is that the events simultaneously exceeded ± one standard deviation of the intensity of the proxy-reconstructed EASM index and the data assimilation-based EASM index over the 1470–2005 CE period. Figure 7b shows that the proxy-reconstructed index and the simulated EASM index have a better correlation after ∼1620 CE. A possible reason is that the number of proxy records has dropped by 43.5% before ∼1620 CE,

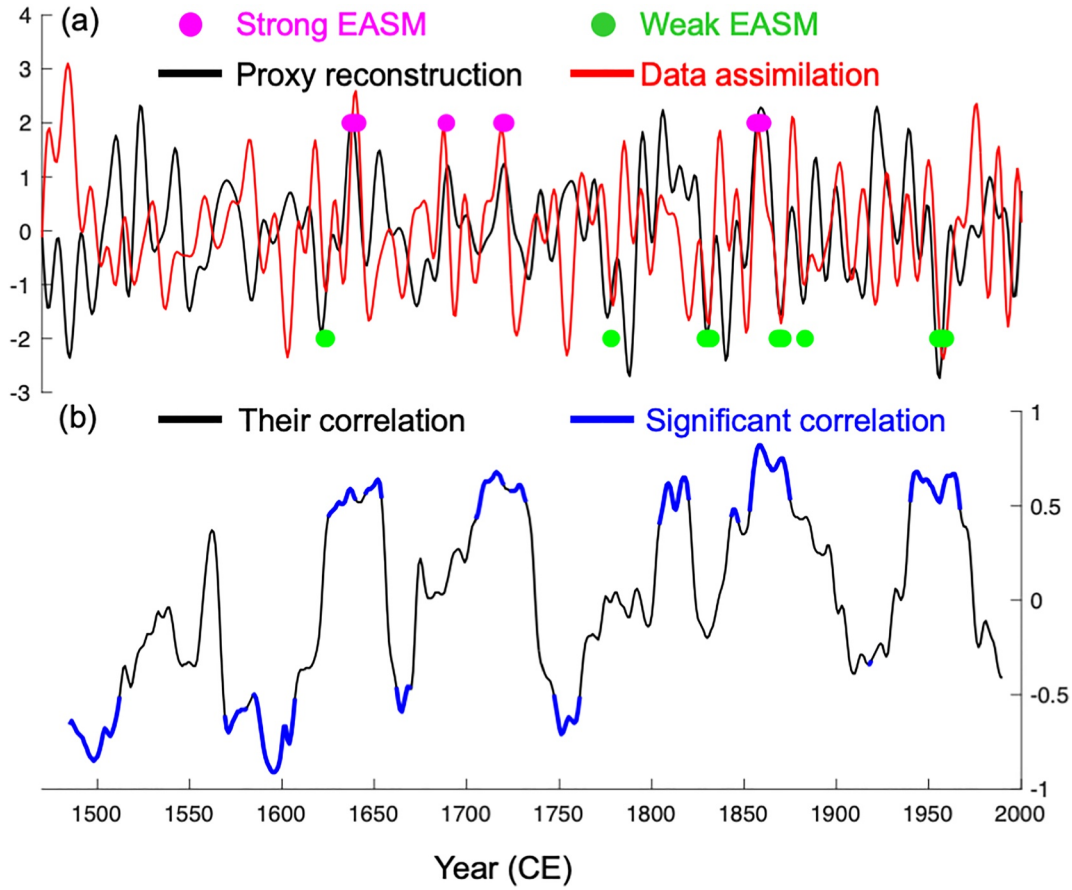

Figure 7. Comparison of the reconstructed East Asian Summer Monsoon (EASM) index (black) with the data assimilation-based EASM index (red) (a), and their 30-year moving correlation (b). The green/magenta points are the events exceeded ± one standard deviation standard deviation of the intensity of these two indices simultaneously over the period 1470–1998 CE. The blue line means that the correlation (black) passes the 90% confidence level.

resulting in a decrease in the proxy reconstruction quality. Likewise, the number of the proxy records used for assimilation decreased by 45.7%, which affected the quality of the data assimilation-based data set.

The proxy reconstructions show that the three components of EASM variability at three timescales (interdecadal, multidecadal, and interdecadal to multidecadal time scales) are significantly negatively correlated with the MJJAS (May–September) precipitation in the middle and lower reaches of the Yangtze River over the 1470–2021 CE period (Figures S1a–S1c in Supporting Information S1), which is consistent with that of the data simulation-based precipitation (Figures S2a–S2c in Supporting Information S1). The reconstructed MJJAS precipitation field as an approximation of JJA precipitation field is used to support the strong correlation between the *Meiyu* precipitation and the proxy reconstructed EASM index. The reason is that there is significant correlation map between the JJA precipitation and the MJJAS precipitation in China at the 99% confidence level (Figure S3 in Supporting Information S1). The negative relationship between the EASM variability and the *Meiyu* precipitation is also found in the composite analysis of the proxy-based MJJAS precipitation field and the data assimilation-based summer (JJA) precipitation field corresponding to the (strong minus weak) EASM case (Figures 8a and 8b). The advantage of the composite analysis using the data-assimilation based reconstruction is that the composited atmospheric circulation is consistent with the features depicted by the data assimilation-based EASM index following the physical laws in the same climate model, and these EASM events also present in the proxy records.

The most robust feature in the data assimilation-based results is a decrease in the summer *Meiyu* precipitation and the prevailing northeasterly wind anomalies in South China (Figure 8b), which is also consistent with the instrumental observations over the period 1958–1999 CE (Li & Zeng, 2002). In addition, this spatial pattern (Figure 8b) is consistent with the first leading mode of the summer precipitation and the three-dimensional

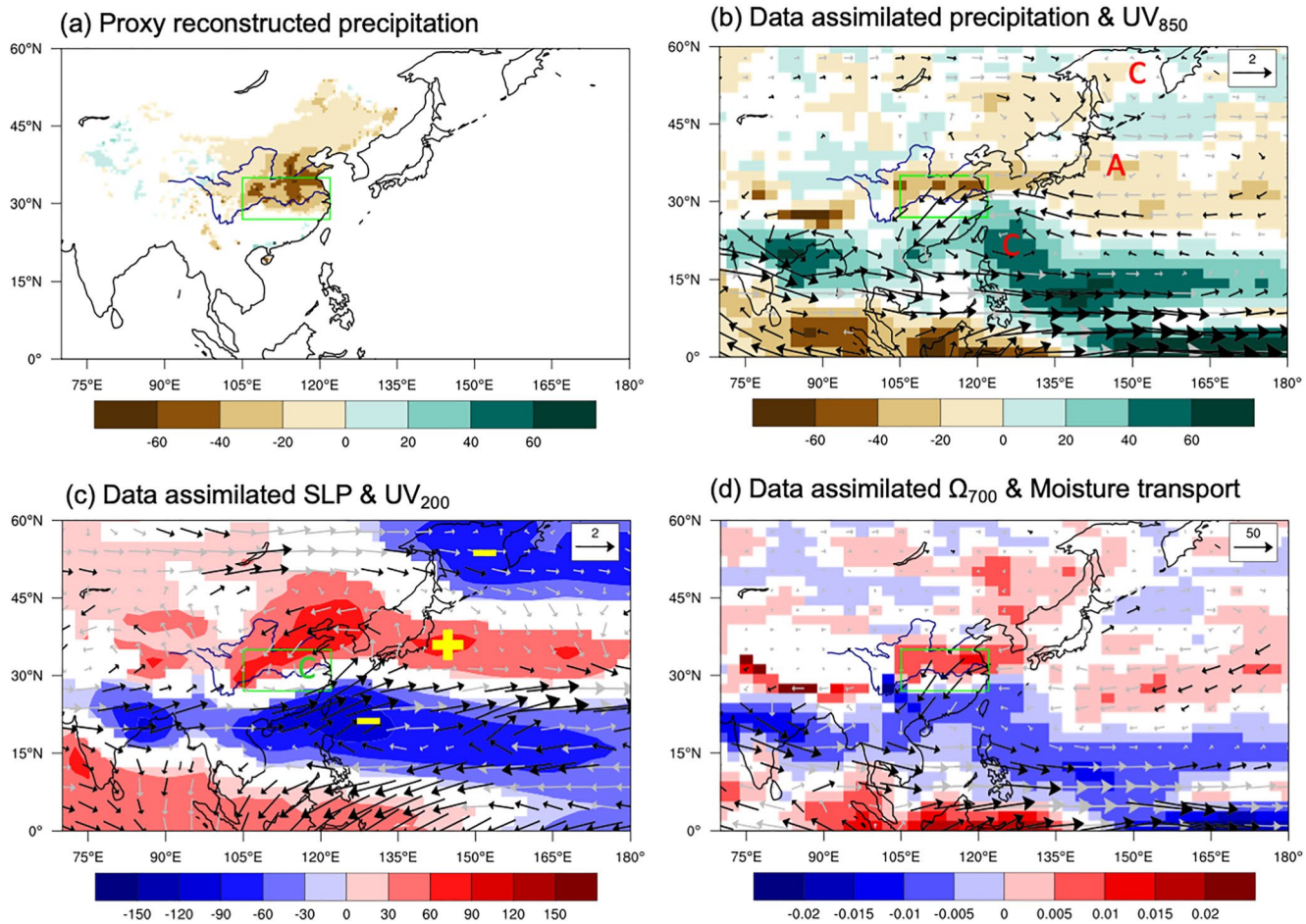

Figure 8. Composite of the reconstructed extended summer (MJJAS) precipitation anomalies (shading) (a), the data assimilation-based summer (JJA) precipitation (shading) and 850-hPa wind anomalies (vector) (b), the data assimilation-based summer sea level pressure (shading, in Pa) and 200-hPa wind anomalies (vector) (c), the reconstructed data assimilation-based summer 700-hPa Omega vertical velocity (Ω, shading) and vertical integral moisture transport (vector) (d) for the 18/15 strong/weak East Asian summer monsoon (EASM) events corresponding to the (weak-strong) EASM case. The white area indicates that the correlation does not exceed the 90% significant level based on a one-tailed Student's *t*-test. The black arrow is the correlation at the 90% significant level based on a one-tailed Student's *t*-test. Gray arrows indicate a one-tailed Student's *t*-test failure. The green box indicates the middle and lower Yangtze River region (27–35°N, 105–122°E) in China. "C"/"A" indicates the cyclonic/anticyclonic anomalies. "–"/"+" indicates the low/high sea level pressure anomalies.

circulation variations associated with EASM through a multivariate empirical orthogonal function analysis (Figure 2a of Wang et al. (2008)), which is often used to measure the EASM strength during the instrumental period 1979–2006 CE. Moreover, this spatial pattern (Figure 8b) is also consistent with the correlation analysis of the data assimilation-based summer (JJA) circulation variations on the three timescales (interdecadal, multidecadal, and interdecadal to multidecadal timescales) (Figures S2a–S2c in Supporting Information S1).

From the composite patterns of the 850/200 hPa wind velocity and the sea level pressure anomalies (Figures 8b and 8c), a zonally elongated cyclonic, anticyclonic, and cyclonic anomalies with centers located around the Philippines-Taiwan, China/the Korean Peninsula/Japan, and East Siberia in the lower troposphere (labeled C, A, and C in Figure 8b); alternating high and low sea level pressure anomalies (labeled –, +, and – in Figure 8c); In the upper troposphere, a cyclone is observed over the middle and lower reaches of the Yangtze River (Figure 8c). This tilted baroclinic structure is favor for the anomalous descending motion from the composite pattern of the 700 hPa vertical velocity anomalies (Figure 8d) and reducing water vapor transport toward the middle and lower reaches of the Yangtze River (Figure 8d). These configurations result in a decreased Meiyu precipitation (Figure 8d). A reduced *Meiyu* precipitation could be associated with the occurrence of a strong EASM, according to the definition of the modern meteorological monsoon research community (Chiang et al., 2020; Li & Zeng, 2002; Wang et al., 2008).

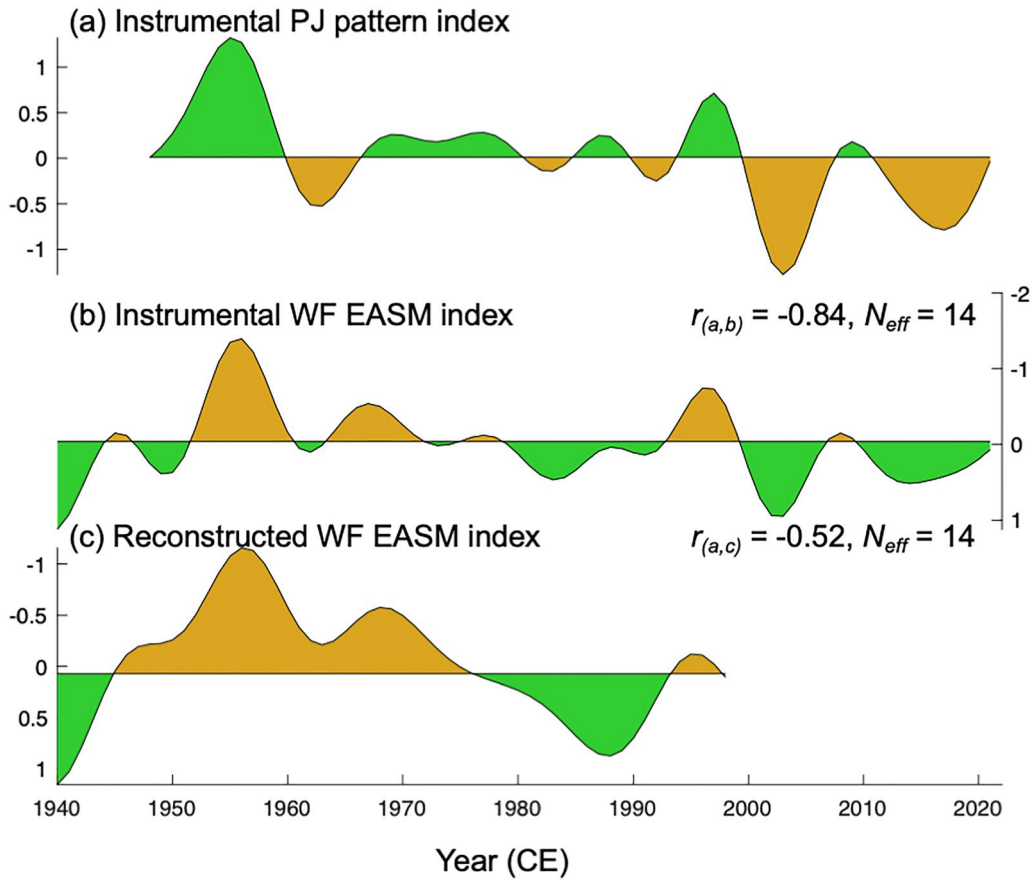

Figure 9. Comparison of the instrumental Pacific-Japan pattern index (a) with the instrumental/reconstructed East Asian Summer Monsoon (EASM) index (b/c) over the interdecadal to multidecadal timescales. *r* is the correlation coefficients during the common period. N_{eff} is the effective degree of freedom in the common period. All correlations are significant at the 90% confidence level based on a one-tailed Student's *t*-test.

There is a meridional alternating positive (15–25°N) and negative (30–40°N) anomaly structure in rainfall anomalies (Figure 8b) and in lower tropospheric circulation (Figure 8c), which are similar to the meridional wave–like teleconnection pattern known as the Pacific-Japan (PJ) pattern/East Asia–Pacific pattern (Huang & Li, 1987; Nitta, 1986; Xie et al., 2016; Xu et al., 2019). This PJ pattern is originally viewed as a poleward propagating Rossby wave train excited by the anomalous convection over the northern Philippines (Huang & Li, 1987; Huang & Sun, 1992; Kosaka & Nakamura, 2006). In addition, the time evolution of the instrumental/reconstructed EASM index is also related to the instrumental PJ index over the interdecadal to multidecadal timescales ($r = -0.84/-0.52$, $n = 14/14$, Figure 9). This implied that there is a strong link between the EASM variability and the PJ-like pattern over the interdecadal to multidecadal timescales before the instrumental period, even though there is no available PJ index reconstruction prior to the instrumental period to test this presumption.

3.3. Position of the Recent 30 years Variability

Figure 6 shows that the interdecadal and multidecadal components of EASM variability during the recent period 1992–2021 CE are not unprecedented over the past half-millennium. Another evidence is derived from the 82 historical analogies of EASM variability over the recent 30 years (1992–2021 CE). The screening criteria of these historical analogies are that the positive and significant correlation and the small RMSE (<1) between the recent 30-year variability (1992–2021 CE) and the other arbitrary 30-year variability over the past 552 years (1470–2021 CE). Results show that the EASM variability over the past 30 years has not exceeded the range of 82 analogies of EASM variability (Figure 10). In addition, the recent 31-year and 51-year variances of EASM variability are lower than that in the late 18 century and the mid 19 century (Figure 11a). This indicates that the recent

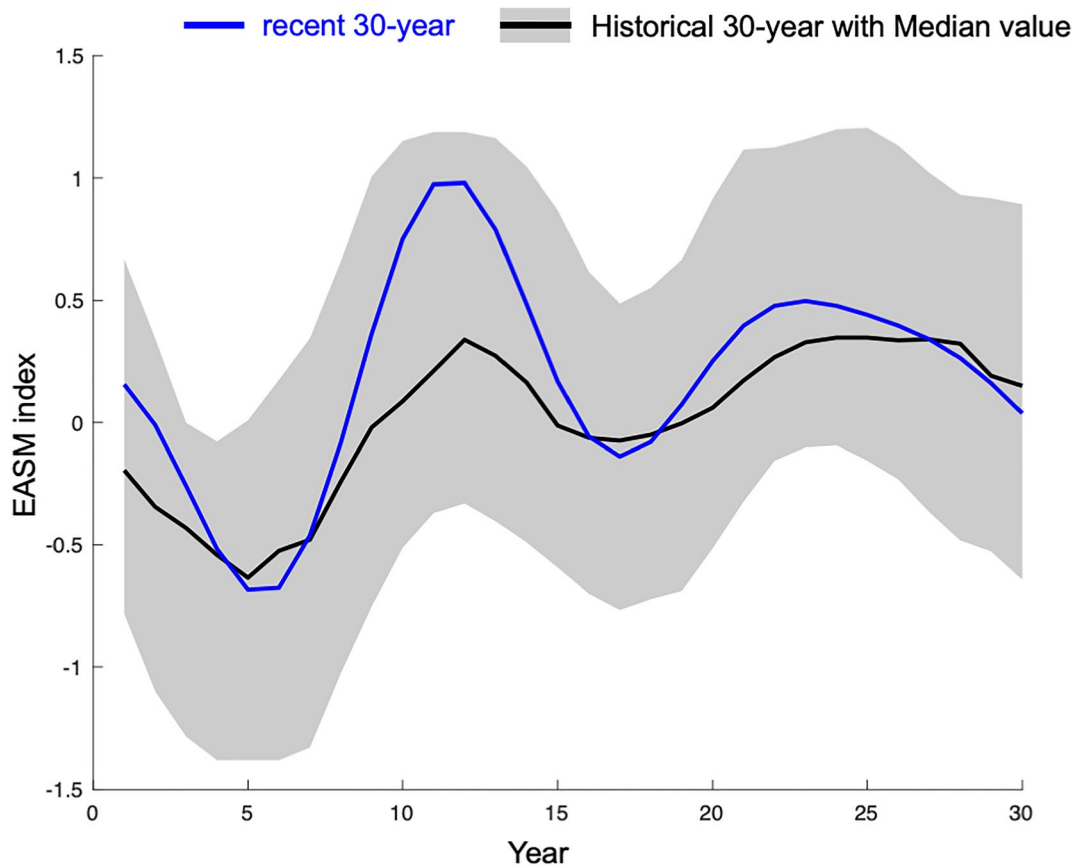

Figure 10. Historical analogies of the East Asian summer monsoon (EASM) variability over the recent 30 years. The blue line is the EASM variability over the past 30 years (1992–2021 CE). The gray borderlines are the 95%/5% quantiles of the 82 historical analogies, and the gray line is the 50% quantiles of the 82 historical analogies.

30-year variability of EASM does not exceed the range of the natural variability, even though the recent EASM variability may still be affected by the anthropogenic aerosols (Z. Li et al., 2016; Liu, Cai et al., 2019). The maximum variance of EASM variability coincides with that of the large volcanic eruptions in Northern Hemisphere in the late 18 century and the early 19 century (Figure 11b). This suggests that the multidecadal climate variability in this period may be instigated by volcanic forcing during this period (Mann et al., 2021; Sun, Liu, et al., 2022).

4. Discussion of the Possible Driving Factor

Previous research in the modern meteorological community indicates the most possible driving factor affecting the EASM variability on interdecadal to multidecadal timescales is the internal sea surface temperature (SST) modes (the Pacific Decadal Oscillation (PDO), the Interdecadal Pacific Oscillation (IPO) and the Atlantic Multidecadal Oscillation (AMO)) through air-sea interactions (An et al., 2015; Shekhar et al., 2022; Wang et al., 2014). The multi-decadal variances of the PDO and the AMO was perhaps significantly intensified by the volcanic forcing during the Little Ice Age (Mann et al., 2021; Sun, Liu, et al., 2022), while the periodicity of the PDO was possibly shortened and its variance is weakened by the GHG forcing in the CMIP5/CMIP6 simulations (Sun, Wang, et al., 2022). We calculated the relationships between the reconstructed EASM index and six reconstructed PDO indices (Biondi et al., 2001; D'Arrigo & Wilson, 2006; Felis et al., 2010; Linsley et al., 2008; MacDonald & Case, 2005; Shen et al., 2006) and two instrumental PDO indices from NOAA Extended Reconstructed SST V5 (Huang et al., 2017) and Mantua et al. (1997), and two reconstructed IPO indices (Porter et al., 2021; Vance et al., 2022) and one instrumental IPO index from NOAA Extended Reconstructed SST V5 (Huang et al., 2017), and two reconstructed AMO indices (Gray et al., 2004; Wang, Yang, et al., 2017) and one instrumental AMO index from Kaplan Extended SST V2 (Kaplan et al., 1998). Through the correlation analysis described above,

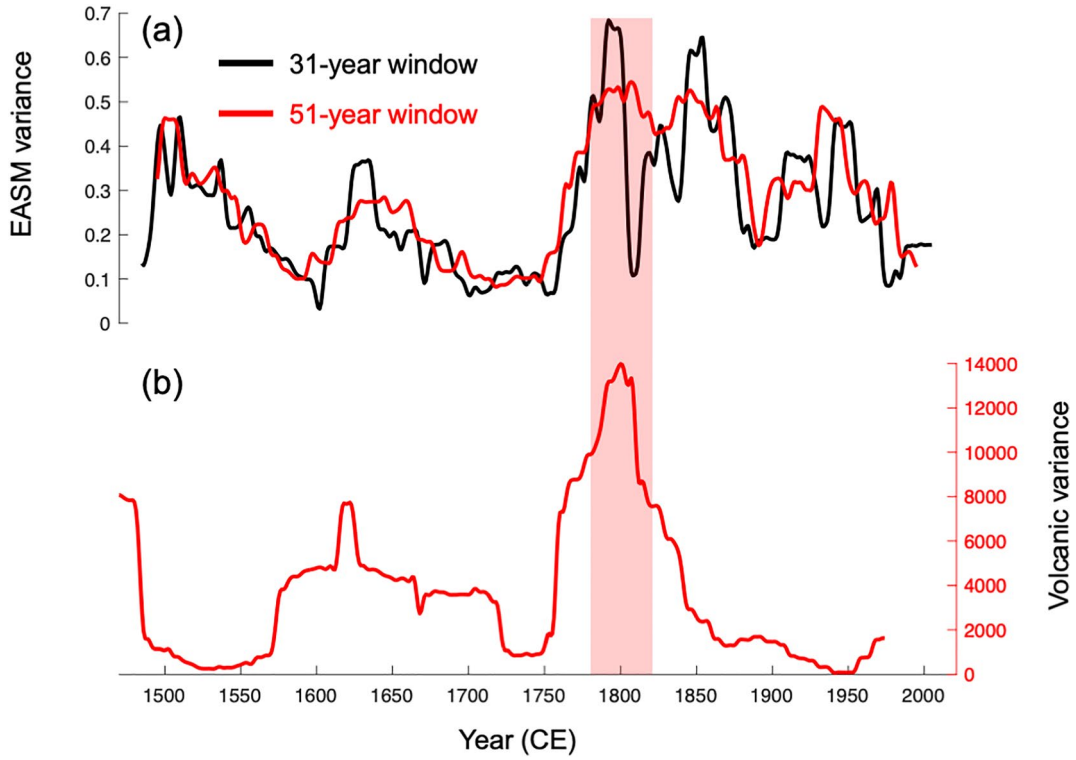

Figure 11. Comparison of the running variances of the reconstructed East Asian summer monsoon index with 31-year (black) and 51-year (red) windows (a) and the volcanic aerosol forcing (V, unit: W m^{-2}) in the Northern Hemisphere with 51-year (red) windows (b). The red shade shows the 1780–1820 CE period. The volcanic aerosol forcing data set is derived from Shi et al. (2022).

the reconstructed EASM index is strongly correlated only with the PDO index over the multidecadal timescale (Figure 12). This suggests that the PDO may trigger the PJ-like pattern on the multidecadal timescale. This is consistent with Wu et al. (2016) during the instrumental period. Meanwhile, the enhanced multi-decadal variability of the PDO during the 1250–1850 CE period is found in the other paleo-assimilation products (LMR) and the CESM-LME simulations (Sun, Liu, et al., 2022). Moreover, the sensitivity experiments have shown that the pattern (similar to the negative PDO) with cooling over the central-eastern tropical Pacific and warming in the extratropical North Pacific and western tropical Pacific can enhance the *Meiyu* precipitation on decadal timescale (Li & Wang, 2018). This occurs via atmosphere-ocean interactions in the extratropical North Pacific and Western tropical Pacific Ocean and can be partly explained by the wind-evaporation/entrainment-SST feedback (Li, Cobb et al., 2017; Wang et al., 2000). Theoretical investigation shows that the zonal gradient of SST across the equatorial Pacific Ocean enhances the easterly anomalies over the Pacific Ocean (Lian et al., 2014). This circulation would strengthen the ascending Walker circulation above the warm pool, and the associated convergence of surface winds piles waters up in the warm pool and lowers sea surface height and SST in the eastern Pacific (Chen, 2011; Lian et al., 2014). The ascending motion of the Walker circulation directly causes the most robust abundant summer (JJA) precipitation anomalies over the Maritime Continent in Southeast Asia and would excite a Rossby wave train to trigger the PJ-like pattern. This results in enhanced southwesterly anomalies in South China and increased *Meiyu* precipitation anomalies, corresponding to a weak EASM.

However, there is no clear relationship between the interdecadal component of EASM variability and the PDO/IPO index over the past half-millennium, even though the decadal variability of the anticyclone in the western North Pacific is linked with the PDO mode (Xie & Wang, 2020), or the IPO mode (Kim & Ha, 2021). A possible reason to understand the non-significant relationship between the interdecadal component of EASM variability and the PDO/IPO index is that the uncertainty of PDO/IPO reconstructions on an interdecadal timescale hampers to exploring of its relationship with the EASM variability. Another possible reason is the long-term phase change/nonstationary of PDO shown in the reconstructions (Figure 10a of Shi and Wang (2019)).

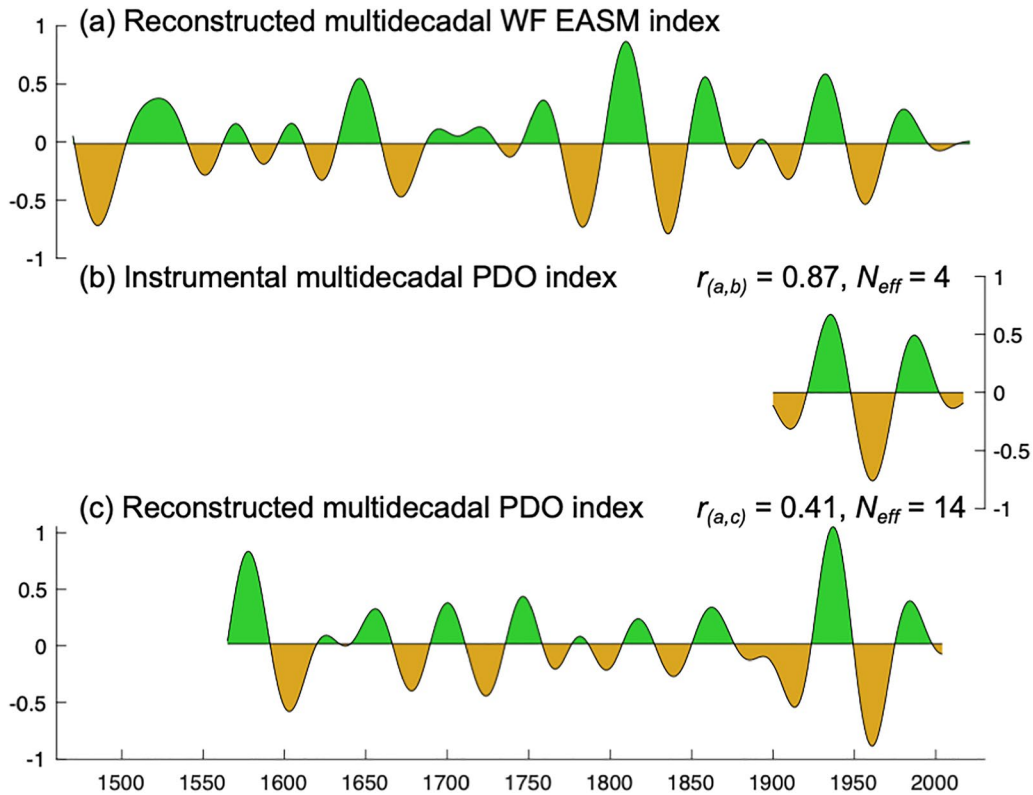

Figure 12. Comparison of the reconstructed East Asian summer monsoon index (a) with the instrumental Pacific Decadal Oscillation (PDO) index (Mantua et al., 1997) (b) and the reconstructed PDO index (D'Arrigo & Wilson, 2006) (c). *r* is the correlation coefficients during the common period. N_{eff} is the effective degree of freedom in the common period. All correlations are significant at the 90% confidence level based on a one-tailed Student's *t*-test.

5. Conclusions

We have reconstructed an EASM circulation index over the past half-millennium (1470–1998 CE) that represents the simultaneous changes of the southwesterly anomalies in South China and the strong *Meiyu* precipitation anomalies in East China under a weak monsoon, the dominant feature of various circulation and precipitation fields in East Asia associated to the EASM. This EASM index extracts the common signal in the three main types of proxy records (including tree-ring, speleothem and historical documentary data) related to EASM. Our major findings are summarized below.

1. Tree-ring and speleothem records do not have consistent signals to represent the monsoon circulation. It means that not all oxygen isotopes records from the tree-rings and the speleothems in East Asia can represent the EASM circulation variability, even though most of the speleothem $\delta^{18}O$ records are negatively correlated with the reconstructed EASM index.
2. Interdecadal to multidecadal variability of EASM over the recent period 1992–2021 CE, and its variance have not exceeded the range of natural variability through 82 historical analogies.
3. The EASM variability on the interdecadal to multidecadal timescales is primarily modulated by the PJ-like teleconnection pattern. In addition, the multidecadal component of the EASM may be linked to the PDO mode through PJ-like pattern.

We believe that the reconstructed EASM index covering the period 1470–1998 CE complements and improves the interdecadal to multidecadal-scale information as compared to previous existing monsoon reconstructions of lower resolution (Wang et al., 2014).

Conflict of Interest

The authors declare no conflicts of interest relevant to this study.

Data Availability Statement

The precipitation reconstruction (IGGPRE.1.0. anom.nc) was archived in the NOAA data repository (https://www.ncdc.noaa.gov/paleo/study/23056), and the CESM-LME model simulation was archived to Climate Data Gateway at NCAR website (https://www.earthsystemgrid.org/dataset/ucar.cgd.ccsm4.CESM_CAM5_LME.html). The reconstructed EASM index was archived at the World Data Center for Geophysics, Beijing (https://doi.org/10.12197/2022GA029).

Acknowledgments

We thank François Klein and Pierre-Yves Barriat for help with the data assimilation. This work was jointly funded by the National Natural Science Foundation of China (Grant 41888101; 41877440; 42077406; 42022059), the Strategic Priority Research Program of Chinese Academy of Sciences (Grant XDB26020000), and the Key Research Program of the Institute of Geology and Geophysics, CAS (Grant IGGCAS-201905). Feng Shi is funded by the Youth Innovation Promotion Association CAS. Hugues Goosse is a Research Director with F.R.S.- FNRS (Belgium). Qiuzhen Yin is Research Associate of F.R.S-FNRS (Belgium). F.C.L. was supported by the Swedish Research Council (Vetenskapsrådet, Grant 2018-01272), and conducted the work with this article as a Pro Futura Scientia XIII Fellow funded by the Swedish Collegium for Advanced Study through Riksbankens Jubileumsfond.

References

Abram, N. J., Mulvaney, R., Vimeux, F., Phipps, S. J., Turner, J., & England, M. H. (2014). Evolution of the southern annular mode during the past millennium. *Nature Climate Change*, *4*, 564–569.

An, W., Liu, X., Leavitt, S. W., Xu, G., Zeng, X., Wang, W., et al. (2014). Relative humidity history on the Batang–Litang Plateau of Western China since 1755 reconstructed from tree-ring δ18O and δD. *Climate Dynamics*, *42*(9–10), 2639–2654. https://doi.org/10.1007/s00382-013-1937-z

An, Z., Wu, G., Li, J., Sun, Y., Liu, Y., Zhou, W., et al. (2015). Global monsoon dynamics and climate change. *Annual Review of Earth and Planetary Sciences*, *43*(1), 29–77. https://doi.org/10.1146/annurev-earth-060313-054623

Biondi, F., Gershunov, A., & Cayan, D. R. (2001). North Pacific decadal climate variability since 1661. *Journal of Climate*, *14*(1), 5–10. https://doi.org/10.1175/1520-0442(2001)014<0005:npdcvs>2.0.co;2

Blasone, R.-S., Vrugt, J. A., Madsen, H., Rosbjerg, D., Robinson, B. A., & Zyvoloski, G. A. (2008). Generalized likelihood uncertainty estimation (GLUE) using adaptive Markov chain Monte Carlo sampling. *Advances in Water Resources*, *31*(4), 630–648. https://doi.org/10.1016/j.advwatres.2007.12.003

Bradley, R. S., & Jones, P. D. (1993). 'Little ice age' summer temperature variations: Their nature and relevance to recent global warming trends. *The Holocene*, *3*(4), 367–376. https://doi.org/10.1177/095968369300300409

Bretherton, C. S., Widmann, M., Dymnikov, V. P., Wallace, J. M., & Bladé, I. (1999). The effective number of spatial degrees of freedom of a time-varying field. *Journal of Climate*, *12*(7), 1990–2009. https://doi.org/10.1175/1520-0442(1999)012<1990:tenosd>2.0.co;2

Cai, Y. J., Tan, L. C., Cheng, H., An, Z. S., Edwards, R. L., Kelly, M. J., et al. (2010). The variation of summer monsoon precipitation in central China since the last deglaciation. *Earth and Planetary Science Letters*, *291*(1–4), 21–31. https://doi.org/10.1016/j.epsl.2009.12.039

Chen, D., Zhou, F., Dong, Z., Zeng, A. Y., Ou, T., & Fang, K. (2020). A tree-ring δ18O based reconstruction of East Asia summer monsoon over the past two centuries. *PLoS One*, *15*(6), e0234421. https://doi.org/10.1371/journal.pone.0234421

Chen, D. K. (2011). Indo-Pacific Tripole: An intrinsic mode of tropical climate variability. *Advances in Geosciences*, *24*, 1–18. https://doi.org/10.1142/9789814355353_0001

Chen, T.-C., & Chen, J.-M. (1995). An observational study of the South China Sea monsoon during the 1979 summer: Onset and life cycle. *Monthly Weather Review*, *123*(8), 2295–2318. https://doi.org/10.1175/1520-0493(1995)123<2295:aosots>2.0.co;2

Chen, W., Wang, L., Feng, J., Wen, Z., Ma, T., Yang, X., & Wang, C. (2019). Recent progress in studies of the variabilities and mechanisms of the East Asian monsoon in a changing climate. *Advances in Atmospheric Sciences*, *36*(9), 887–901. https://doi.org/10.1007/s00376-019-8230-y

Cheng, H., Edwards, R. L., Sinha, A., Spötl, C., Yi, L., Chen, S., et al. (2016). The Asian monsoon over the past 640, 000 years and ice age terminations. *Nature*, *534*(7609), 640–646. https://doi.org/10.1038/nature18591

Chiang, J. C. H., Herman, M. J., Yoshimura, K., & Fung, I. Y. (2020). Enriched East Asian oxygen isotope of precipitation indicates reduced summer seasonality in regional climate and westerlies. *Proceedings of the National Academy of Sciences*, *117*(26), 14745–14750. https://doi.org/10.1073/pnas.1922602117

Chinese Academy of Meteorological Science, C. M. A. (1981). *Yearly charts of dryness/wetness in China for the last 500-year period*. Cartological Press.

Christiansen, B. (2011). Reconstructing the NH mean temperature: Can underestimation of trends and variability be avoided? *Journal of Climate*, *24*(3), 674–692. https://doi.org/10.1175/2010jcli3646.1

Danis, P.-A., Hatté, C., Misson, L., & Guiot, J. (2012). MAIDENiso: A multiproxy biophysical model of tree-ring width and oxygen and carbon isotopes. *Canadian Journal of Forest Research*, *42*(9), 1697–1713. https://doi.org/10.1139/x2012-089

D'Arrigo, R., & Wilson, R. (2006). On the Asian expression of the PDO. *International Journal of Climatology*, *26*(12), 1607–1617. https://doi.org/10.1002/joc.1326

Ding, Y., Li, C., & Liu, Y. (2004). Overview of the South China Sea monsoon experiment. *Advances in Atmospheric Sciences*, *21*(3), 343–360. https://doi.org/10.1007/bf02915563

Ding, Y., Wang, Z., & Sun, Y. (2008). Inter-decadal variation of the summer precipitation in East China and its association with decreasing Asian summer monsoon. Part I: Observed evidences. *International Journal of Climatology*, *28*(9), 1139–1161. https://doi.org/10.1002/joc.1615

Duan, W., Ruan, J., Luo, W., Li, T., Tian, L., Zeng, G., et al. (2016). The transfer of seasonal isotopic variability between precipitation and drip water at eight caves in the monsoon regions of China. *Geochimica et Cosmochimica Acta*, *183*, 250–266. https://doi.org/10.1016/j.gca.2016.03.037

Dubinkina, S., Goosse, H., Sallaz-Damaz, Y., Crespin, E., & Crucifix, M. (2011). Testing a particle filter to reconstruct climate changes over the past centuries. *International Journal of Bifurcation and Chaos*, *21*(12), 3611–3618. https://doi.org/10.1142/s0218127411030763

Felis, T., Suzuki, A., Kuhnert, H., Rimbu, N., & Kawahata, H. (2010). Pacific decadal oscillation documented in a coral record of North Pacific winter temperature since 1873. *Geophysical Research Letters*, *37*(14), L14605. https://doi.org/10.1029/2010gl043572

Field, R. D., Andreu-Hayles, L., D'arrigo, R. D., Oelkers, R., Luckman, B. H., Morimoto, D., et al. (2022). Tree-ring cellulose δ18O records similar large-scale climate influences as precipitation δ18O in the Northwest Territories of Canada. *Climate Dynamics*, *58*(3–4), 759–776. https://doi.org/10.1007/s00382-021-05932-4

Fritsch, F. N., & Carlson, R. E. (1980). Monotone piecewise cubic interpolation. *SIAM Journal on Numerical Analysis*, *17*(2), 238–246. https://doi.org/10.1137/0717021

Fritts, H. (1976). *Tree rings and climate*. The Blackburn Press.
Ge, Q., Guo, X., Zheng, J., & Hao, Z. (2008). Meiyu in the middle and lower reaches of the Yangtze River since 1736. *Chinese Science Bulletin*, *53*(1), 107–114. https://doi.org/10.1007/s11434-007-0440-5
Gray, S. T., Graumlich, L. J., Betancourt, J. L., & Pederson, G. T. (2004). A tree-ring based reconstruction of the Atlantic multidecadal oscillation since 1567 AD. *Geophysical Research Letters*, *31*(12), L12205. https://doi.org/10.1029/2004gl019932
Hu, C., Henderson, G. M., Huang, J., Xie, S., Sun, Y., & Johnson, K. R. (2008). Quantification of Holocene Asian monsoon rainfall from spatially separated cave records. *Earth and Planetary Science Letters*, *266*(3–4), 221–232. https://doi.org/10.1016/j.epsl.2007.10.015
Huang, B., Thorne, P. W., Banzon, V. F., Boyer, T., Chepurin, G., Lawrimore, J. H., et al. (2017). Extended reconstructed sea surface temperature, version 5 (ERSSTv5): Upgrades, validations, and intercomparisons. *Journal of Climate*, *30*(20), 8179–8205. https://doi.org/10.1175/jcli-d-16-0836.1
Huang, R., Chen, J., Wang, L., & Lin, Z. (2012). Characteristics, processes, and causes of the spatio-temporal variabilities of the East Asian monsoon system. *Advances in Atmospheric Sciences*, *29*(5), 910–942. https://doi.org/10.1007/s00376-012-2015-x
Huang, R., & Sun, F. (1992). Impacts of the tropical Western Pacific on the east Asian summer monsoon. *Journal of the Meteorological Society of Japan Ser. II*, *70*(1B), 243–256. https://doi.org/10.2151/jmsj1965.70.1b_243
Huang, R. H., & Li, W. J. (1987). Influence of the heat source anomaly over the Western tropical Pacific on the subtropical high over East Asia. In *Proceedings of the international conference on the general circulation of East Asia* (pp. 40–51).
Kaplan, A., Cane, M. A., Kushnir, Y., Clement, A. C., Blumenthal, M. B., & Rajagopalan, B. (1998). Analyses of global sea surface temperature 1856-1991. *Journal of Geophysical Research*, *103*(C9), 18567–18589. https://doi.org/10.1029/98jc01736
Kim, S., & Ha, K.-J. (2021). Interannual and decadal covariabilities in East Asian and Western North Pacific summer rainfall for 1979–2016. *Climate Dynamics*, *56*(3–4), 1017–1033. https://doi.org/10.1007/s00382-020-05517-7
Kosaka, Y., & Nakamura, H. (2006). Structure and dynamics of the summertime Pacific–Japan teleconnection pattern. *Quarterly Journal of the Royal Meteorological Society*, *132*(619), 2009–2030. https://doi.org/10.1256/qj.05.204
Lavergne, A., Gennaretti, F., Risi, C., Daux, V., Boucher, E., Savard, M. M., et al. (2017). Modelling tree ring cellulose δ18O variations in two temperature-sensitive tree species from North and South America. *Climate of the Past*, *13*(11), 1515–1526. https://doi.org/10.5194/cp-13-1515-2017
Li, J., & Wang, B. (2018). Origins of the decadal predictability of East Asian land summer monsoon rainfall. *Journal of Climate*, *31*(16), 6229–6243. https://doi.org/10.1175/jcli-d-17-0790.1
Li, J., Wang, B., & Yang, Y.-M. (2020). Diagnostic metrics for evaluating model simulations of the east Asian monsoon. *Journal of Climate*, *33*(5), 1777–1801. https://doi.org/10.1175/jcli-d-18-0808.1
Li, J., & Zeng, Q. (2002). A unified monsoon index. *Geophysical Research Letters*, *29*(8), 115-1–115-4. https://doi.org/10.1029/2001gl013874
Li, M., Huang, C., Hinnov, L., Ogg, J., Chen, Z.-Q., & Zhang, Y. (2016). Obliquity-forced climate during the early triassic hothouse in China. *Geology*, *44*(8), 623–626. https://doi.org/10.1130/g37970.1
Li, Q., Nakatsuka, T., Kawamura, K., Liu, Y., & Song, H. (2011). Regional hydroclimate and precipitation δ18O revealed in tree-ring cellulose δ18O from different tree species in semi-arid Northern China. *Chemical Geology*, *282*(1–2), 19–28. https://doi.org/10.1016/j.chemgeo.2011.01.004
Li, T., Wang, B., Wu, B., Zhou, T., Chang, C.-P., & Zhang, R. (2017a). Theories on formation of an anomalous anticyclone in Western north Pacific during El Niño: A review. *Journal of Meteorological Research*, *31*(6), 987–1006. https://doi.org/10.1007/s13351-017-7147-6
Li, X., Cheng, H., Tan, L., Ban, F., Sinha, A., Duan, W., et al. (2017b). The East Asian summer monsoon variability over the last 145 years inferred from the Shihua Cave record, North China. *Scientific Reports*, *7*(1), 7078. https://doi.org/10.1038/s41598-017-07251-3
Li, Z., Lau, K. M., Ramanathan, V., Wu, G., Ding, Y., Manoj, M. G., et al. (2016). Aerosol and monsoon climate interactions over Asia: Aerosol and monsoon climate interactions. *Reviews of Geophysics*, *54*(4), 866–929. https://doi.org/10.1002/2015rg000500
Lian, T., Chen, D. K., Tang, Y. M., & Jin, B. G. (2014). A theoretical investigation of the tropical Indo-Pacific tripole mode. *Science China Earth Sciences*, *57*(1), 174–188. https://doi.org/10.1007/s11430-013-4762-7
Linsley, B. K., Zhang, P., Kaplan, A., Howe, S. S., & Wellington, G. M. (2008). Interdecadal-decadal climate variability from multicoral oxygen isotope records in the South Pacific Convergence Zone region since 1650 A.D. Paleoceanography (Vol. *23*).
Liu, H., Zhou, T., Zhu, Y., & Lin, Y. (2012). The strengthening East Asia summer monsoon since the early 1990s. *Chinese Science Bulletin*, *57*(13), 1553–1558. https://doi.org/10.1007/s11434-012-4991-8
Liu, Y., Cai, W., Sun, C., Song, H., Cobb, K. M., Li, J., et al. (2019). Anthropogenic aerosols cause recent pronounced weakening of Asian summer monsoon relative to last four centuries. *Geophysical Research Letters*, *46*(10), 5469–5479. https://doi.org/10.1029/2019gl082497
Liu, Y., Cobb, K. M., Song, H., Li, Q., Li, C.-Y., Nakatsuka, T., et al. (2017). Recent enhancement of central Pacific El Niño variability relative to last eight centuries. *Nature Communications*, *8*(1), 15386. https://doi.org/10.1038/ncomms15386
Liu, Y., Liu, H., Song, H., Li, Q., Burr, G. S., Wang, L., & Hu, S. (2017). A monsoon-related 174-year relative humidity record from tree-ring δ18O in the Yaoshan region, eastern central China. *Science of the Total Environment*, *593–594*, 523–534. https://doi.org/10.1016/j.scitotenv.2017.03.198
Liu, Y., Wang, L., Li, Q., Cai, Q., Song, H., Sun, C., et al. (2019). Asian Summer monsoon-related relative humidity recorded by tree ring δ18O during last 205 years. *Journal of Geophysical Research: Atmospheres*, *124*(17–18), 9824–9838. https://doi.org/10.1029/2019jd030512
Liu, Z., Wen, X., Brady, E. C., Otto-Bliesner, B., Yu, G., Lu, H., et al. (2014). Chinese cave records and the East Asia Summer Monsoon. *Quaternary Science Reviews*, *83*, 115–128. https://doi.org/10.1016/j.quascirev.2013.10.021
Lyu, Z., Goosse, H., Dalaiden, Q., Klein, F., Shi, F., Wagner, S., & Braconnot, P. (2021). Spatial patterns of multi–centennial surface air temperature trends in Antarctica over 1–1000 CE: Insights from ice core records and modeling. *Quaternary Science Reviews*, *271*, 107205. https://doi.org/10.1016/j.quascirev.2021.107205
MacDonald, G. M., & Case, R. A. (2005). Variations in the Pacific decadal oscillation over the past millennium. *Geophysical Research Letters*, *32*(8), L08703. https://doi.org/10.1029/2005gl022478
Mann, M. E., Park, J., & Bradley, R. (1995). Global interdecadal and century-scale climate oscillations during the past five centuries. *Nature*, *378*(6554), 266–270. https://doi.org/10.1038/378266a0
Mann, M. E., Steinman, B. A., Brouillette, D. J., & Miller, S. K. (2021). Multidecadal climate oscillations during the past millennium driven by volcanic forcing. *Science*, *371*(6533), 1014–1019. https://doi.org/10.1126/science.abc5810
Mann, M. E., Zhang, Z. H., Hughes, M. K., Bradley, R. S., Miller, S. K., Rutherford, S., & Ni, F. B. (2008). Proxy-based reconstructions of hemispheric and global surface temperature variations over the past two millennia. *Proceedings of the National Academy of Sciences of the United States of America*, *105*(36), 13252–13257. https://doi.org/10.1073/pnas.0805721105
Mantua, N. J., Hare, S. R., Zhang, Y., Wallace, J. M., & Francis, R. C. (1997). A Pacific interdecadal climate oscillation with impacts on salmon production. *Bull. Am. Meteorol. Soc.*, *78*(6), 1069–1079. https://doi.org/10.1175/1520-0477(1997)078<1069:apicow>2.0.co;2

Mizukoshi, M. (1993). Climatic reconstruction in central Japan during the Little Ice Age based on documentary sources. *Journal of Geography*, *102*(2), 152–166. https://doi.org/10.5026/jgeography.102.2_152

Nakatsuka, T., Sano, M., Li, Z., Xu, C., Tsushima, A., Shigeoka, Y., et al. (2020). A 2600-year summer climate reconstruction in central Japan by integrating tree-ring stable oxygen and hydrogen isotopes. *Climate of the Past*, *16*(6), 2153–2172. https://doi.org/10.5194/cp-16-2153-2020

Neukom, R., Barboza, L. A., Erb, M. P., Shi, F., Emile-Geay, J., Evans, M. N., et al. (2019). Consistent multidecadal variability in global temperature reconstructions and simulations over the Common Era. *Nature Geoscience*, *12*(8), 643–649. https://doi.org/10.1038/s41561-019-0400-0

Nitta, T. (1986). Long-term variations of cloud amount in the Western Pacific region. *Journal of the Meteorological Society of Japan Ser. II*, *64*(3), 373–390. https://doi.org/10.2151/jmsj1965.64.3_373

Ortega, P., Lehner, F., Swingedouw, D., Masson-Delmotte, V., Raible, C. C., Casado, M., & Yiou, P. (2015). A model-tested North Atlantic oscillation reconstruction for the past millennium. *Nature*, *523*(7558), 71–74. https://doi.org/10.1038/nature14518

Otto-Bliesner, B. L., Brady, E. C., Fasullo, J., Jahn, A., Landrum, L., Stevenson, S., et al. (2016). Climate variability and change since 850 C.E.: An ensemble approach with the Community Earth System Model (CESM). *Bulletin of the American Meteorological Society*, *97*, 735–754.

Porter, S. E., Mosley-Thompson, E., Thompson, L. G., & Wilson, A. B. (2021). Reconstructing an interdecadal Pacific oscillation index from a Pacific basin–wide collection of ice core records. *Journal of Climate*, *34*(10), 3839–3852. https://doi.org/10.1175/jcli-d-20-0455.1

Roden, J. S., Lin, G., & Ehleringer, J. R. (2000). A mechanistic model for interpretation of hydrogen and oxygen isotope ratios in tree-ring cellulose. *Geochimica et Cosmochimica Acta*, *64*(1), 21–35. https://doi.org/10.1016/s0016-7037(99)00195-7

Sano, M., Xu, C., & Nakatsuka, T. (2012). A 300-year Vietnam hydroclimate and ENSO variability record reconstructed from tree ring $\delta^{18}O$. *Journal of Geophysical Research*, *117*(D12), D12115. https://doi.org/10.1029/2012jd017749

Seo, J.-W., Sano, M., Jeong, H.-M., Lee, K.-H., Park, H.-C., Nakatsuka, T., & Shin, C.-S. (2019). Oxygen isotope ratios of subalpine conifers in Jirisan National Park, Korea and their dendroclimatic potential. *Dendrochronologia*, *57*, 125626. https://doi.org/10.1016/j.dendro.2019.125626

Shekhar, M., Sharma, A., Dimri, A. P., & Tandon, S. K. (2022). Asian summer monsoon variability, global teleconnections, and dynamics during the last 1, 000 years. *Earth-Science Reviews*, *230*, 104041. https://doi.org/10.1016/j.earscirev.2022.104041

Shen, C., Wang, W. C., Gong, W., & Hao, Z. (2006). A Pacific Decadal Oscillation record since 1470 AD reconstructed from proxy data of summer rainfall over eastern China. *Geophysical Research Letters*, *33*(3), L03702. https://doi.org/10.1029/2005gl024804

Shi, F., Duan, A., Yin, Q., Bruun, J. T., Xiao, C., & Guo, Z. (2021). Modulation of the relationship between summer temperatures in the Qinghai–Tibetan Plateau and Arctic over the past millennium by external forcings. *Quaternary Research*, *103*, 130–138. https://doi.org/10.1017/qua.2021.3

Shi, F., Fang, K., Xu, C., Guo, Z., & Borgaonkar, H. P. (2017). Interannual to centennial variability of the South Asian summer monsoon over the past millennium. *Climate Dynamics*, *49*(7–8), 2803–2814. https://doi.org/10.1007/s00382-016-3493-9

Shi, F., Goosse, H., Klein, F., Zhao, S., Liu, T., & Guo, Z. (2019). Monopole mode of precipitation in East Asia modulated by the South China Sea over the last four centuries. *Geophysical Research Letters*, *46*(24), 14713–14722. https://doi.org/10.1029/2019gl085320

Shi, F., Li, J., & Wilson, R. J. S. (2014). A tree-ring reconstruction of the South Asian summer monsoon index over the past millennium. *Scientific Reports*, *4*(1), 6739. https://doi.org/10.1038/srep06739

Shi, F., Sun, C., Guion, A., Yin, Q., Zhao, S., Liu, T., & Guo, Z. (2022). Roman warm period and late antique little ice age in an Earth system model large ensemble. *Journal of Geophysical Research: Atmospheres*, *127*(16), e2021JD035832. https://doi.org/10.1029/2021jd035832

Shi, F., Yang, B., Charpentier Ljungqvist, F., & Fengmei, Y. (2012). Multi-proxy reconstruction of Arctic summer temperatures over the past 1400 years. *Climate Research*, *54*(2), 113–128. https://doi.org/10.3354/cr01112

Shi, F., Yang, B., Linderholm, H. W., Seftigen, K., Yang, F., Yin, Q., et al. (2020). Ensemble standardization constraints on the influence of the tree growth trends in dendroclimatology. *Climate Dynamics*, *54*(7–8), 3387–3404. https://doi.org/10.1007/s00382-020-05179-5

Shi, F., Yang, B., Mairesse, A., von Gunten, L., Li, J., Bräuning, A., et al. (2013). Northern Hemisphere temperature reconstruction during the last millennium using multiple annual proxies. *Climate Research*, *56*(3), 231–244. https://doi.org/10.3354/cr01156

Shi, F., Zhao, S., Guo, Z., Goosse, H., & Yin, Q. (2017). Multi-proxy reconstructions of May–September precipitation field in China over the past 500 years. *Climate of the Past*, *13*(12), 1919–1938. https://doi.org/10.5194/cp-13-1919-2017

Shi, H., & Wang, B. (2019). How does the Asian summer precipitation-ENSO relationship change over the past 544 years? *Climate Dynamics*, *52*(7–8), 4583–4598. https://doi.org/10.1007/s00382-018-4392-z

Sun, C., Liu, Y., Li, Q., Song, H., Cai, Q., Fang, C., et al. (2021). Tree rings reveal the impacts of the northern Hemisphere temperature on precipitation reduction in the low latitudes of East Asia since 1259 CE. *Journal of Geophysical Research: Atmospheres*, *126*(7), e2020JD033603. https://doi.org/10.1029/2020jd033603

Sun, W., Liu, J., Wang, B., Chen, D., & Gao, C. (2022). Pacific multidecadal (50–70 year) variability instigated by volcanic forcing during the Little Ice Age (1250–1850). *Climate Dynamics*, *59*(1–2), 231–244. https://doi.org/10.1007/s00382-021-06127-7

Sun, W., Wang, B., Liu, J., & Dai, Y. (2022). Recent changes of Pacific decadal variability shaped by greenhouse forcing and internal variability. *Journal of Geophysical Research: Atmosphere*, *127*(8), e2021JD035812. https://doi.org/10.1029/2021jd035812

Tan, L., Cai, Y., Cheng, H., Edwards, L. R., Lan, J., Zhang, H., et al. (2018). High resolution monsoon precipitation changes on southeastern Tibetan Plateau over the past 2300 years. *Quaternary Science Reviews*, *195*, 122–132. https://doi.org/10.1016/j.quascirev.2018.07.021

Tan, L., Li, Y., Wang, X., Cai, Y., Lin, F., Cheng, H., et al. (2020). Holocene monsoon change and abrupt events on the Western Chinese loess plateau as revealed by accurately dated stalagmites. *Geophysical Research Letters*, *47*(21), e2020GL090273. https://doi.org/10.1029/2020gl090273

Tan, L. C., Cai, Y. J., An, Z. S., Edwards, R. L., Cheng, H., Shen, C. C., & Zhang, H. W. (2010). Centennial-to decadal-scale monsoon precipitation variability in the semi-humid region, northern China during the last 1860 years: Records from stalagmites in Huangye Cave. *The Holocene*, *21*(2), 287–296. https://doi.org/10.1177/0959683610378880

Tingley, M. P., & Huybers, P. (2010). A bayesian algorithm for reconstructing climate anomalies in space and time. Part I: Development and applications to paleoclimate reconstruction problems. *Journal of Climate*, *23*(10), 2759–2781. https://doi.org/10.1175/2009jcli3015.1

Vaganov, E. A., Anchukaitis, K. J., & Evans, M. N. (2011). How well understood are the processes that create dendroclimatic records? A mechanistic model of the climatic control on conifer tree-ring growth dynamics. In M. K. Hughes, T. W. Swetnam, & H. F. Diaz (Eds.), *Dendroclimatology: Progress and prospects* (pp. 37–75). Springer Netherlands.

Vance, T. R., Kiem, A. S., Jong, L. M., Roberts, J. L., Plummer, C. T., Moy, A. D., et al. (2022). Pacific decadal variability over the last 2000 years and implications for climatic risk. *Communications Earth & Environment*, *3*(1), 33. https://doi.org/10.1038/s43247-022-00359-z

van Leeuwen, P. J. (2009). Particle filtering in geophysical systems. *Monthly Weather Review*, *137*(12), 4089–4114. https://doi.org/10.1175/2009mwr2835.1

Vega, I., Gallego, D., Ribera, P., de Paula Gomez-Delgado, F., Garcia-Herrera, R., Pena-Ortiz, C., et al. (2018). Reconstructing the Western north Pacific summer monsoon since the late nineteenth century. *Journal of Climate*, *31*(1), 355–368. https://doi.org/10.1175/jcli-d-17-0336.1

Wang, B., & Fan, Z. (1999). Choice of South Asian summer monsoon indices. *Bulletin of the American Meteorological Society*, *80*(4), 629–638. https://doi.org/10.1175/1520-0477(1999)080<0629:cosasm>2.0.co;2

Wang, B., Jhun, J.-G., & Moon, B.-K. (2007). Variability and singularity of Seoul, South Korea, rainy season (1778–2004). *Journal of Climate*, *20*(11), 2572–2580. https://doi.org/10.1175/jcli4123.1

Wang, B., Wu, R., & Fu, X. (2000). Pacific–East Asian teleconnection: How does ENSO affect east Asian climate? *Journal of Climate*, *13*(9), 1517–1536. https://doi.org/10.1175/1520-0442(2000)013<1517:peathd>2.0.co;2

Wang, B., Wu, R., & Lau, K. (2001). Interannual variability of the Asian summer monsoon: Contrasts between the Indian and the Western north Pacific-east Asian monsoons. *Journal of Climate*, *14*(20), 4073–4090. https://doi.org/10.1175/1520-0442(2001)014<4073:ivotas>2.0.co;2

Wang, B., Wu, Z., Li, J., Liu, J., Chang, C.-P., Ding, Y., & Wu, G. (2008). How to measure the strength of the east Asian summer monsoon. *Journal of Climate*, *21*(17), 4449–4463. https://doi.org/10.1175/2008jcli2183.1

Wang, H. (2001). The weakening of the Asian monsoon circulation after the end of 1970's. *Advances in Atmospheric Sciences*, *18*(3), 376–386. https://doi.org/10.1007/bf02919316

Wang, J., Yang, B., Ljungqvist, F. C., Luterbacher, J., Osborn, T. J., Briffa, K. R., & Zorita, E. (2017). Internal and external forcing of multidecadal Atlantic climate variability over the past 1, 200 years. *Nature Geoscience*, *10*(7), 512–517. https://doi.org/10.1038/ngeo2962

Wang, P., Wang, B., Cheng, H., Fasullo, J., Guo, Z., Kiefer, T., & Liu, Z. (2014). The global monsoon across time scales: Is there coherent variability of regional monsoons? *Climate of the Past Discussions*, *10*(6), 2007–2052. https://doi.org/10.5194/cp-10-2007-2014

Wang, Y., Chen, S., Xu, K., Yan, L., Yue, X., He, F., & Wei, Y. (2021). Ancient auroral records compiled from Korean historical books. *Journal of Geophysical Research: Space Physics*, *126*(1), e2020JA028763. https://doi.org/10.1029/2020ja028763

Wang, Y., Cheng, H., Edwards, R. L., He, Y., Kong, X., An, Z., et al. (2005). The holocene Asian monsoon: Links to solar changes and North Atlantic climate. *Science*, *308*(5723), 854–857. https://doi.org/10.1126/science.1106296

Wang, Z., Hoffmann, T., Six, J., Kaplan, J. O., Govers, G., Doetterl, S., & Van Oost, K. (2017). Human-induced erosion has offset one-third of carbon emissions from land cover change. *Nature Climate Change*, *7*(5), 345–349. https://doi.org/10.1038/nclimate3263

Wu, B., Zhou, T., & Li, T. (2016). Impacts of the Pacific–Japan and circumglobal teleconnection patterns on the interdecadal variability of the east Asian summer monsoon. *Journal of Climate*, *29*(9), 3253–3271. https://doi.org/10.1175/jcli-d-15-0105.1

Xie, M., & Wang, C. (2020). Decadal variability of the anticyclone in the Western north Pacific. *Journal of Climate*, *33*(20), 9031–9043. https://doi.org/10.1175/jcli-d-20-0008.1

Xie, S.-P., Kosaka, Y., Du, Y., Hu, K., Chowdary, J. S., & Huang, G. (2016). Indo-Western Pacific ocean capacitor and coherent climate anomalies in post-ENSO summer: A review. *Advances in Atmospheric Sciences*, *33*(4), 411–432. https://doi.org/10.1007/s00376-015-5192-6

Xu, C., Ge, J., Nakatsuka, T., Yi, L., Zheng, H., & Sano, M. (2016). Potential utility of tree ring δ18O series for reconstructing precipitation records from the lower reaches of the Yangtze River, southeast China. *Journal of Geophysical Research: Atmospheres*, *121*(8), 3954–3968. https://doi.org/10.1002/2015jd023610

Xu, C., Pumijumnong, N., Nakatsuka, T., Sano, M., & Li, Z. (2015). A tree-ring cellulose δ18O-based July–October precipitation reconstruction since AD 1828, northwest Thailand. *Journal of Hydrology*, *529*, 433–441. https://doi.org/10.1016/j.jhydrol.2015.02.037

Xu, C., Sano, M., & Nakatsuka, T. (2013). A 400-year record of hydroclimate variability and local ENSO history in northern Southeast Asia inferred from tree-ring δ18O. *Palaeogeography, Palaeoclimatology, Palaeoecology*, *386*, 588–598. https://doi.org/10.1016/j.palaeo.2013.06.025

Xu, C., Zhao, Q., An, W., Wang, S., Tan, N., Sano, M., et al. (2021). Tree-ring oxygen isotope across monsoon Asia: Common signal and local influence. *Quaternary Science Reviews*, *269*, 107156. https://doi.org/10.1016/j.quascirev.2021.107156

Xu, C., Zheng, H., Nakatsuka, T., & Sano, M. (2013). Oxygen isotope signatures preserved in tree ring cellulose as a proxy for April–September precipitation in Fujian, the subtropical region of southeast China. *Journal of Geophysical Research: Atmospheres*, *118*(23), 12805–12815. https://doi.org/10.1002/2013jd019803

Xu, P., Wang, L., Chen, W., Feng, J., & Liu, Y. (2019). Structural changes in the Pacific–Japan pattern in the late 1990s. *Journal of Climate*, *32*(2), 607–621. https://doi.org/10.1175/jcli-d-18-0123.1

Yang, B., Qin, C., Bräuning, A., Osborn, T. J., Trouet, V., Ljungqvist, F. C., et al. (2021). Long-term decrease in Asian monsoon rainfall and abrupt climate change events over the past 6, 700 years. *Proceedings of the National Academy of Sciences*, *118*(30), e2102007118. https://doi.org/10.1073/pnas.2102007118

Yang, B., Qin, C., Wang, J., He, M., Melvin, T. M., Osborn, T. J., & Briffa, K. R. (2014). A 3, 500-year tree-ring record of annual precipitation on the northeastern Tibetan Plateau. *Proceedings of the National Academy of Sciences of the United States of America*, *111*(8), 2903–2908. https://doi.org/10.1073/pnas.1319238111

Zhang, D. (1991). Historical records of climate change in China. *Quaternary Science Reviews*, *10*(6), 551–554. https://doi.org/10.1016/0277-3791(91)90049-z

Zhang, D., Li, H.-C., Ku, T.-L., & Lu, L. (2010). On linking climate to Chinese dynastic change: Spatial and temporal variations of monsoonal rain. *Chinese Science Bulletin*, *55*(1), 77–83. https://doi.org/10.1007/s11434-009-0584-6

Zhang, D. E., & Wang, P. K. (1991). A study on the reconstruction of the eighteenth century Meiyu (Plum rains) activity of lower Changjiang (Yangtze) region of China. *Science in China Series B*, *34*, 1237–1245.

Zhang, P., Cheng, H., Edwards, R., Chen, F., Wang, Y., Yang, X., et al. (2008). A test of climate, sun, and culture relationships from an 1810-year Chinese cave record. *Science*, *322*(5903), 940–942. https://doi.org/10.1126/science.1163965

Zheng, J., Hao, Z., & Ge, Q. (2005). Variation of precipitation for the last 300 years over the middle and lower reaches of the Yellow River. *Science in China - Series D: Earth Sciences*, *48*(12), 2182–2193. https://doi.org/10.1360/03yd0392

Zhou, T., Gong, D., Li, J., & Li, B. (2009). Detecting and understanding the multi-decadal variability of the East Asian summer monsoon recent progress and state of affairs. *Meteorologische Zeitschrift*, *18*(4), 455–467. https://doi.org/10.1127/0941-2948/2009/0396